Scientific report; 97 - 05

KNMI

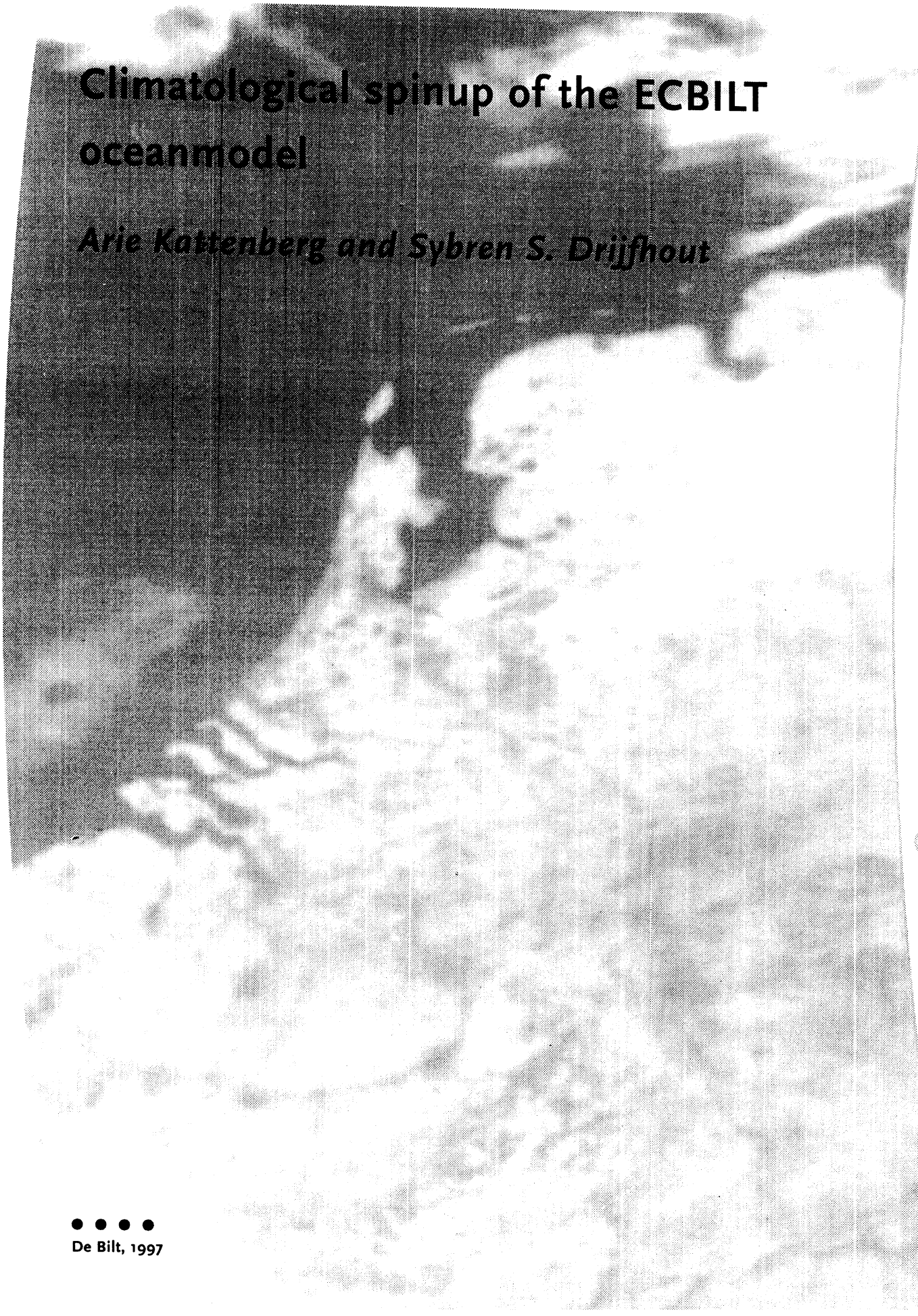

Climatological spinup of the ECBILT oceanmodel

Arie Kattenberg and Sybren S. Drijfhout

Koninklijk Nederlands Meteorologisch Instituut

De Bilt, 1997

Scientific report = wetenschappelijk rapport; WR 97 - 05

De Bilt, 1997

P.O. Box 201
3730 AE De Bilt
Wilhelminalaan 10
Telefoon 030-220 69 11
telefax 030-221 04 07

Authors: A. Kattenberg and
S.S. Drijfhout

UDC: 551.465.5
551.583
551.556.8

ISSN: 0169-1651

ISBN: 90-369-2123 -6

● ● ● ●

Climatological spinup of the ECBILT oceanmodel

(Arie Kattenberg and Sybren S. Drijfhout)

ABSTRACT

In the present WR we evaluate a 4000 year spinup of the ocean component of the KNMI ECBILT coupled climate model. The simulation was forced by monthly mean observed windstress data and by relaxation towards observed monthly mean climatological SST and SSS data. Goal of the experiment was to assess the performance of the stand alone OGCM in order to have a reference for further experiments in which the OGCM is part of a coupled system.

Our conclusions are that the model works properly and as intended: relevant processes such as thermohaline and wind driven circulations are operating and relevant structures such as the main global watermasses and thermocline are present, all qualitatively similar to observations. Quantitatively, the climatological state of the model is somewhat less satisfactory, compared to other OGCMs of comparable costs. We hypothesise that most of the deficiencies are related to the flat bottom and simplified equation of state.

1 Introduction

Our KNMI research group investigates climate variability at interyearly and decadal timescales using a coupled atmosphere-ocean model (named ECBILT, Opsteegh et al., 1997). In this report we focus on the Ocean General Circulation Model component which was developed to be of intermediate complexity and low computational cost. The aim of this report is to investigate the climatology of the OGCM when forced with climatological windstress and heat- and freshwater forcing in order to assess it's performance.

This study consists of a short description of the ocean component of the ECBILT coupled climate model and an evaluation of the mean state of the ocean model in a stand-alone configuration, driven by observed mean climatological winds and relaxation towards observed SST and SSS. Furthermore, this study is an assessment of the performance of the ocean component with respect to other global OGCMs, in particular with the Hamburg LSG (Maier-Reimer et al., 1993).

In section 2 we discuss the experimental setup, with descriptions of the model, forcing data and model parameters. In section 3 results are presented in terms of water masses, flow patterns and transports. Section 4 presents a discussion of the results and summarises the conclusions that emerge from this invesigation.

2 Experimental setup

To get a notion of the 'degree of realism' of the ocean model's simulations, we force it for a long time with (observed) monthly climatological data and inspect the resulting 'climate equilibrium'. Before we can do that, however, we had to select values for free parameters, for which we made several short simulations with the model. Also we had to circumnavigate problems with the sea-ice model that is incorporated in the coupled ocean-atmosphere model, that is, sea-ice thickness in the Arctic does not reach equilibrium but is still increasing after O(1000 yr).

Ocean Model

The OGCM is a primitive equation model, discretised on a geographical (locally cartesian - Arakawa B) grid, with $5.625° \times 5.625°$ horizontal resolution and 12 layers in the vertical; these layers are spaced tens of meters near the surface, with increasing layer thickness towards the flat bottom at 4000 m depth. The OGCM is essentially a flat bottom derivate of the GFDL ocean model (e.g., Bryan 1969, Bryan and Lewis, 1979, Toggweiler et al., 1989, England, 1993).

In the present model the hydrostatic approximation and rigid lid assumption have been made. An equation of state has been used that is quadratic in temperature and linear in salinity dependence, ignoring pressure dependence.

The momentum equation is split in a barotropic and a baroclinic part. The barotropic mode is determined diagnostically as an equilibrium response to the windstress. The baro-

clinic mode is stepped in time. Heat and salt are advected horizontally using a leapfrog method, while forward timestepping is used for diffusion and vertical advection.

Convective adjustment is implemented in the usual manner: Starting at the surface, pairs of vertically adjacent boxes are checked for stratification and completely mixed when unstable stratification is found.

Forcing data

To impart momentum into the oceans, we used the Hellerman & Rosenstein (1983) monthly mean surface stress fields, re-gridded from it's $2° \times 2°$ origin onto the vector points of the $5.625° \times 5.625°$ Arakawa type-B grid of the ocean model. The sea surface salinity was relaxed towards Levitus (1982) salinities (yearly mean climatology). In one experiment the temperature was relaxed towards COADS SST (Woodruff et al. 1987), in a second experiment the temperature was relaxed to the COADS surface air temperature data (in both cases monthly mean climatologies, interpolated to daily values). Where surface air temperatures were used, an additional 'mean shortwave flux' parameterized as a function of day of year and latitude in a simple fashion by E. Maier-Reimer (personal communication) was used, see also Drijfhout et al. 1996.

Model parameters

A number of parameters in the model, related to parameterisations of physical processes, are not rigourously fixed either by theoretical considerations or by observations. These can be used to control and 'tune' the working of the ocean model. No attempt was made to find 'optimal' settings for these parameters, as it is well known that such choices are dependent on each other and on the exact form of the boundary conditions that are applied. We performed, however, several preliminary experiments with different choices for some parameters, to obtain an indication of the sensitivity of the model results to these parameters in the present experimental setup.

internal mixing

Small scale mixing and diffusion is parameterized in the model using k-theory. The mixing coëfficient in the horizontal (*'rkaph'*) has a value of 1000 m^2s^{-1}. We verified that doubling the value of this parameter led to warmer and more saline conditions in the simulated deep ocean. Decreasing the vertical mixing coëfficient *'rkapv'* from 0.003 m^2s^{-1} to 0.0001 m^2s^{-1} led to warmer and *less* saline conditions in the deep ocean.

air sea interaction

Heat and freshwater forcing of the ocean was accomplished by relaxation of the two uppermost layers (thickness 80 m) towards observed climatological values. The timescales for these relaxation processes were chosen after an exploration of several combinations of values

with relatively short (400 yr) runs and comparison of the resulting salinities and temperatures and their tendencies. For freshwater forcing a timescale of 60 days seemed to yield the best results; for temperature relaxation the timescale was chosen 20 days when relaxating to SST's and 60 days when relaxing to surface air temperatures. In the latter case an adittional 'shortwave' heat flux has been used to prevent the ocean from cooling. Also a sea-ice model was added to describe thermodynamics when the atmosphere induces cooling of sea water to temperatures below -1.9 degrees Celsius.

Sea-ice

The formation, transport and melting of sea-ice are important processes relevant for (deep) water formation. A sea-ice cover has both a strong (thermally) insulating effect and a strong albedo effect. Moreover, brine rejection and transport of sea-ice between it's formation and its melting result in climatologically relevant freshwaterfluxes associated with sea-ice. We have tested the influence of a representation of sea-ice in an explicit form, by including a simple thermodynamic sea-ice model, based on Semtner's zero layer model (1976). In order to force the sea-ice model, surface air temperatures and a mean shortwave flux were applied.

In preliminary tests, sea ice that grows in the model Arctic ocean showed a tendency to grow perpetually or at least on a timescale of hundreds of years.

Experiments

To avoid numerical instability in high latitudes, where meridians converge and grid boxes become small, the oceans North of 70°N are represented by a diffusive 'swamp' type ocean. Probably due to the limited heat transport capacity of this polar swamp, the sea-ice model showed a drift in ice thickness in the arctic. This drift resulted in perpetually growing sea-ice there, without the ice thickness reached equilibrium. To avoid this problem, we made our definitive, 4000 yr run twice; one without an ice model altogether, restoring SST to observed values; the other with an ice model which was only active in the Southern Hemisphere and restoring to COADS air temperatures.

Two 4000 year integrations were made with the model in the configuration and with the momentum and freshwater forcings described above. The run with no ice model was forced with COADS SST everywhere. The second run had the sea ice model in the Southern Hemisphere only. In this run the temperature was forced with surface air temperatures and a parameterisation for short wave radiation; freshwater forcing under the ice was done by the ice model rather than by relaxation towards climatology. North of 60°N, the temperature forcing was by relaxation to COADS SSTs, as in the first run. Only moderate differences are apparent in the model's response during these runs, and in the following we mainly describe the run with sea ice in the Southern Hemisphere.

The results are compared to the performance of state-of-the-art OGCMs in use in climate research and with observations. We focus our comparisons on the Large Scale Geostrophic model (LSG) of the Max Planck Institut für Meteorologie in Hamburg (Maier-Reimer et al.,

1993), which is has a comparable cost of operation to the ECBILT model.

3 Results

Water properties

The globally averaged profiles of temperature and salinity in the two long spinup experiments are compared with observations in Figure 1. Even stronger than many coarse resolution climate ocean circulation models, the deep ocean temperatures have a warm bias of a few degrees Celsius. The surface temperatures, which are strongly constrained by the relaxation towards observed temperatures, are similar to the observations.

In the temperature profiles, the model thermocline is less sharp than in the observations, and the discrepancy between the model and the observations is largest ($\sim$ 3.5°C) directly beneath the thermocline at about 1000 m depth. England (1993) demonstrates that a state-of-the-art OGCM (the GFDL model) with bottom topography and slightly finer resolution (3.75° $\times$ 4.5°) can be tuned to show a global mean temperature bias of at most 1.5 – 2°C. The globally averaged salinity is also biased most strongly ($\sim$ 0.03 psu) in the seasonal thermocline between 500 and 1500 m. In terms of density the salinity bias compensates the thermal bias partly.

The bias in the density field is not uniform over the oceans. We compare the density structure along the GEOSECS (Bainbridge, 1981) sections in the West Atlantic (Fig. 2a,c,e) and Mid Pacific (Fig. 2b,d,f) oceans, with Levitus (1982) data, and sections from the Hamburg LSG model. At 1000 m depth, the waters in the (sub)tropical Western North Atlantic have a density bias of 0.6–0.7 kg/m^3. The deeper NADW with an observed density (σ_0) of 27.8 kg/m^3, has σ_0 = 27.3 kg/m^3 in the model simulation. In the Pacific the water at 1000 m depth is 0.5–0.6 kg/m^3 too light. The 'common water' that makes up the body of Pacific Ocean water has a σ_0 of 27.5 kg/m^3 in the model and 27.7 in the observations. In the deep ocean the density bias is everywhere 0.1 – 0.2 kg/m^3. The density biases are an order of magnitude larger in this model than in the LSG model. Another systematic error is that both in the Pacific and in the Atlantic the isopycnals near 60° N and S are much too steeply inclined.

Salinity profiles along the GEOSECS sections (Figs. 3a,c and e) show some agreement with observations and the LSG model (Figs. 3b,d and f). In particular the 35 psu isohaline in the model West Atlantic, shows the imprint of northward flowing AAIW between 500 and 1500 m depth, southward flowing NADW between 1500 and 3000 m and a hint of fresher, northward flowing AABW below, similar to observations. The model AAIW, with salinity between 34.5 and 35 psu is saltier than in the real ocean (34.4 to 34.8 psu). NADW, with salinity between 35 and 35.5 psu, is also too salty (34.9 to 35 psu in the observations). The salinity of the model AABW (between 34.7 and 34.9 psu) is similar to observations.

Convection

The average potential energy release due to convection is shown in figure 4. Although bottom-, deep- and intermediate water formation is taking place, we notice, when comparing with state-of-the-art OGCMs, e.g. LSG (Maier-Reimer et al., 1993) (not shown), some deficiencies that are apparent: Too much intermediate water is being formed. The main water formation near the Antarctic takes place about 5-10 degrees northward of the location where AABW should be formed, in the shallow coastal Ross- and Weddell seas. Intermediate water formation in the south Indian and North West Pacific is much more vigourous in this model than in LSG (or reality, presumably). The Deep water formation in the North Atlantic occurs in roughly the same area as in the LSG, but the Labrador Sea water production is weaker and the GIN Sea water production is stronger than in the LSG model.

Circulation and overturning

The horizontal flow in the surface layer is shown in Figure 5a. Geostrophic flow and ekman-drift reproduce the observed gyre circulations and boundary currents (though much wider and slower than in reality) qualitatively. The barotropic streamfunction (Figure 6) shows the Antarctic Circumpolar Current with 100 Sv transport (prescribed in the model) and gyre circulations of 10–20 Sv in the Northern Hemisphere and a few Sv in the Southern Hemisphere. The (non-prescribed) barotropic circulation in the simulation is rather weak: The Northern Hemisphere gyres are roughly a factor of two weaker, those in the Southern Hemisphere four to five times weaker than in the LSG model. The subpolar gyre in the north Atlantic cannot be represented due to the 'swamp type ocean' north of 70° N. As can be expected from a coarse resolution model, several detailed features, like The North Equatorial Counter Current and the Brazil Current are lacking from the simulation. At a depth of 2000 m (Fig. 5c) the outflow of NADW from the northern North Atlantic Ocean can be seen as well as equatorward eastern boundary currents in the other basins that make up the deep branches of the 'conveyor belt'. In the bottom circulation (Fig. 5d), inflow of AABW into the Pacific and Atlantic basins can be seen. A deep counterflow in the model AAC, which gives it a baroclinic structure contrary to observation, is related to the numerical technique in which the total barotropic transport in the ACC is prescribed. It augments deficiencies in the watermass properties in the southern regions of the model.

The meridional overturning in the modelbasins is shown in Figure 7. The Atlantic basin shows the source of NADW with sinking of 24 Sv at 70° N. Though this overturning is of a magnitude similar to observations, much of this water wells up to the surface again between 50 and 60° N in the model, leaving only 12 Sv NADW which flows out into the southern Atlantic basin at a depth of 1000 m. In the real ocean some upwelling does occur, but further to the south, and more of the water is connected with the global conveyor circulation. Underneath the southward NADW flow a counterflow of about 3 Sv of model AABW crosses the equator, which seems reasonable. Similar to observations, the Pacific overturning shows the signature of the conveyor circulation with inflow of a few Sv (a factor of three less than in the LSG model) from the south along the bottom, of water that upwells

between 30° S and 30° N. The Southern ocean shows a narrow overturning cell of 10 Sv (one third of that in the LSG model) adjacent to the Antarctic Continent, in assocation with the sinking and formation of AABW. Between 40 and 60° S a strongly developed 'Deacon cell' of 25 Sv is present, which reaches much too deep.

Transports

heat

Figure 8 shows the basin and global meridional heat transports, compared to the HOPE OGCM (Drijfhout et al., 1996) and the LSG OGCM from the Max Plack Institut für Meteorologie in Hamburg. The meridional heat transport in the Atlantic basin is similar in shape, but about half the magnitude of that in the LSG and HOPE models. The Pacific heat transport in the Northern Hemisphere is very similar to that of the other GCMs. The Southern Hemisphere meridional heattransport in the Pacific is, however, about a factor 3 smaller than that in the Hamburg models. The simulated heat transport in the Indian ocean basin is similar to that in the HOPE model, and a factor of two weaker than in the LSG model. Southern Ocean meridional heat transport is again underestimated by a factor of 3, relative to the Hamburg GCMs.

The total surface heat exchange (compared to that of the LSG and HOPE models in Figure 9) presents another view on how the physical mechanisms are operating in the model. Regions of water mass formation show up as 'hot spots' where strong cooling leads to (deep) convection. The hot spot associated with NADW formation at 70° N in the Greenland, Iceland Norwegian sea is similar to that in the HOPE model. The signals of AABW formation, however, near the Weddell and Ross seas in the Antarctic region, are much smaller in the ECBILT model than in the HOPE climatology. In stead, two prominent hot spots are found just north of the ACC, at 40° S, SE of the continents of Africa and Australia in our model. These indicate a vigorous formation of 'intermediate water', (AAIW) in the model. Intermediate- and mode water formation in the North Pacific also seems rather strong, as indicated by the hot spot near the Kuroshio (extension), which is more than four times as strong in this model compared to the HOPE model.

freshwater

The meridional freshwater transport (Figure 10) is about a factor of three too strong, compared to the HOPE and LSG models. Also, the total flux is not balanced, consistent with the freshening trend in the simulated deep ocean. Figure 11 shows that the patterns of the surface freshwaterflux (playing the role of 'precipitation - evaporation' in the forcing strategy) are similar to but rather stronger than those in the LSG model.

4 Discussion and Conclusions

The climatological transports, watermass distribution and 'air sea interaction' in the ECBILT ocean model, forced with climatological windstressses and simple relaxation towards temperature and salinity fields, are reminiscent to observations, but with much too diffuse a structure and a severe underestimate of the meridional heat transport and wind driven gyre transport, especially in the Southern Hemisphere. The thermohaline circulation, however, with NADW outflow out of the Atlantic into the world ocean and a warm water return flow into the Atlantic is of the right order of magnitude. Such a result may be typical and reasonable for a coarse resolution, flat bottom OGCM, but it is worse in quality than those of state-of-the-art OGCMs like HOPE and LSG. Characteristic is the lack of sharp gradients, such as the seasonal thermocline or the western boundary currents of the gyre circulations. Concurrently, there is a warm temperature bias and a positive salinity bias, both strongest between 500 and 1500 m.

The deficiencies of the model are not uniformly distributed over the globe, and they can be traced back to failures in the representation of key processes due to the integration on a coarse resolution (locally) cartesian grid, a flat bottom and a simplified equation of state. We highlight several areas where problems arise.

NADW outflow

The amount of 'NADW' that is sinking in the model North Atlantic ocean ($\sim$ 24 Sv – see Figure 7a) is reasonable. The outflow of NADW towards the South Atlantic (12 Sv instead of $\sim$ 16–18 Sv) is rather small and much (up to 5°C) too warm. In Figure 7a it can be seen that the water which has sunk at 70° N rises again south of 65° N, due to mixing with warmer and fresher water there. At those latitudes, the isopycnals in the model are very steeply inclined, especially in the upper layers between 1500 m and the surface (see Figure 2a,c and e). The effective horizontal diffusion, partly explicit in the model and partly as a spurious result of the advection scheme, is much stronger than cross isopycnal transport can be in the real ocean. Therefore a spurious horizontal heat flow across the nearly vertical isopycnals in the model will be set up. Figure 11a, the zonally averaged meridional heatflux in the model Atlantic, shows spurious advective transport between 30 and 60° N at 200 – 700 m depth. At the same location we see a strong temperature anomaly in the zonally averaged Atlantic temperatures (Figure 12b); The isotherms bulge downward and northward. The spurious heat that accumulates will have two effects: The surface waters flowing towards the sinking region will be warmed and the sinking will be less deep. Also the southward flowing NADW will be warmed. Part of this upwelling water that is warmed crosses the thermocline from beneath and enters isopycnal layers that outcrop at 60 to 70° N. It no longer flows southward, but it stagnates and eventually flows northward, to participate again in the sinking motion.

Thus deficiencies concerning NADW in the model (too little and too warm) are associated with indications of too strong diapycnal mixing in the region of the 'polar front'.

Intermediate water

Severe underestimation of the meridional heat transport in the Southern Hemisphere oceans (Fig. 8) is a conspicuous 'symptom' of another set of problems in the model. We already indicated the very steep isopycnals in the South Pacific part of the GEOSECS section (Fig. 2a) and we indicated in figure 8 the spurious 'hot spots' in the surface heat exchange of the model, associated with intermediate or mode water formation. The steep isopycnals and isothermals can be seen as resulting from the presence of 'much too much' intermediate water, or AAIW, PIW and subtropical mode water, which fills the lower latitude basins to a great depth. At the same time the meridional heat transport is 'short circuited'; the poleward heat transport associated with the formation of deep water at high latitudes is weak, especially in the Southern Hemisphere where AABW formation is much too small and spurious intermediate water production is vigourous.

Southern Ocean and AABW

Figure 13 shows the zonally averaged temperature and salinity structure in the ACC. Similar to the situation with NADW, most of the AABW that sinks along the Antarctic continent rises again at adjacent latitudes (Fig. 7c), heated by spurious heat transport through the vertical isopycnals there. This circulation is shielded from the atmosphere by a freshwater layer (Fig. 13b). The AAC has a baroclinic structure in this model, with a westward counterflow near the bottom, which mixes and transports the AABW in the model erroneously. The result is a diminished flow of AABW into the Pacific and Atlantic basins.

Sea-ice

Figure 14 shows the mean sea-ice cover in the Southern Hemisphere. Interaction with convection and stratification gives rise to some variability in the simulations on the interannual to decadal timescales, which we do not expect to be realistic. Both the extent and the thickness of the mean sea-ice cover are reasonably realistic on the large spatial scale, but the model has a tendency to accumulate too much ice in the Ross- and Weddell Seas which is not observed. Brine rejected from this ice will influence watermass qualities in the Southern ocean. As a result, the SSS in the Southern Ocean is too high: $\sim$ 34.5 ppt rather than $\sim$ 33.8.

Conclusions

The ECBILT primitive equation Ocean General Circulation Model that was tested here, performs satisfactory in the stand-alone version. Compared to the Hamburg LSG model, which has similar cost of operation, however, the model performs less well. Within the coupled ECBILt model (Opsteegh et al., 1997) the OGCM's climatology is strongly influenced by climate drift of the coupled system. The conclusions about its main deficiencies, however, remain unchanged. The climatological state demonstrates that the model works properly

and as intended: relevant processes such as thermohaline and wind driven circulation are operating, and relevant structures such as watermasses and thermocline are present, all qualitatively similar to observations. Quantitatively, however, and when looking in more detail, the climatological state of the model is less satisfactory: The middle and deep oceans are much too warm; the relative rates of formation of and the amount of inflow of various watermasses are wrong, with too much intermediate water replacing deep and bottom waters that are also too warm and deficient in quantity. (Surface) circulation is too weak, especially in the Southern Hemisphere. The same holds for the meridional heat transport which is also too weak, especially in the Southern Hemisphere. The E-P fluxes needed to maintain observed SSS are too strong everywhere. Most of the deficiencies in the circulation of deep- and bottom waters seem to be related to the flat bottom and simplified equation of state.

Though the model was designed to have a fast performance (hence e.g. the flat ocean bottom), its numerical solution method imposes fundamental limits on the timestep, which cannot be chosen longer than one day. The Hamburg-LSG model, on the contrary, can be operated with a timestep of 30 days (due to an implicit formulation of the advection from which the non-linear part is ignored). Therefore, the LSG, which is more complex and sophisticated than the ECBILT OGCM and which yields a better climatological state, outperforms it. We recommend that the LSG OGCM will be implemented into the next ECBILT cycle.

References

Bainbridge, A.E., 1981: GEOSECS Atlantic expedition. Vol. 2: Sections and profiles. U.S. Govt. Printing Office, Washington, D.C., Stock No. 038-000-00435-2.

Bryan, K., 1969: A Numerical Method for the Study of the Circualtion of the World Ocean, *J. Comput. Physics*, **4**, 347 - 376.

Bryan, K., and L.J. Lewis, 1979: A Water Mass Model of the World Ocean, *J. Geophys. Res.*, **84**, 2503-2517.

Drijfhout, S., C. Henze, M. Latif and E. Maier-Reimer, 1996: Mean Circulation and Internal Variability in an Ocean Primitive Equation Model, *J. Phys. Oceanogr.*, **26**, 559 - 580.

England, M.H., 1993: Representing the Global Scale Water Masses in Ocean General Circulation Models, *J. Phys. Oceanogr.*, **23**, 1523 - 1552.

Hasselmann, K., 1976: Stochastic Climate Models. Part I: Theory, *Tellus*, **28**, 473 - 485.

Hellerman, S. and M. Rosenstein, 1983: Normal monthly wind stress over the World Ocean with error estimates, *J. Phys. Oceanogr.*, **13**, 1093 - 1104.

Levitus, S. 1982: Climatological Atlas of the World Ocean, NOAA Prof. Paper No. 13, U.S. Govt. Printing Office, 173 pp.

Maier-Reimer, E., U. Mikolajewicz and K. Hasselmann, 1993: Mean Circulation of the Hamburg LSG OGCM and its Sensitivity to the Thermohaline Surface forcing, *J. Phys. Oceanogr.*, **23**, 731 - 757.

Opsteegh, J.D., R.J. Haarsma, F.M. Selten, and A. Kattenberg, 1997: ECBILT, an Atmospheric Model of Intermediate Complexity: an Alternative to Mixed Boundary Conditions in Ocean Models, *Tellus, submitted.*

Semtner, A.J., 1976: A model for the thermodynamic growth of sea-ice in numerical investigations of climate., *J. Phys. Oceanogr.*, **6**, 379 - 389.

Toggweiler, J.R., K. Dixon, and K. Bryan, 1989: Simulations of Radiocarbon in a Course-resolution World Ocean Model. 1. Steady State Prebomb Distribution, *J. Geophys. Res.*, **94**, 8217 - 8242.

Woodruff, S.D., R.J. Slutz, R.L. Jenne and P.M. Steurer, 1987: A comprehensive ocean-atmosphere dataset., *Bull. Amer. Meteor. Soc.*, **68**, 1239 - 1250.

Figures

1. Globally averaged profiles of temperature (a) and salinity (b), compared with Levitus (1982) observed data.

2. Density (σ_θ) along GEOSECS sections (Bainbridge 1981) in the West Atlantic (a) and mid-Pacific (b), compared to the LSG model (c and d) and to observations (Levitus 1982) (e and f).

3. Salinity along along GEOSECS sections (Bainbridge 1981) in the West Atlantic (a) and mid-Pacific (b), compared to the LSG model (c and d) and to observations (Levitus 1982) (e and f).

4. Mean potential energy release by convection

5. Horizontal flow vectors in modellayers at the surface (a), 230 m (b), 2000 m (c) and near the bottom at 3700 m (d).

6. Barotropic streamfunction of the World Ocean (a), compared to the LSG model (b).

7. Meridional overturning streamfunction in the Atlantic, Pacific and World Ocean for ECBILT (resp. a,b,c) and HOPE (resp. d,e,f)

8. Meridional heat transport (a) compared to LSG (b) and HOPE (c).

9. Surface heat exchange (a) compared to the HOPE model (b).

10. Meridional freshwater transport (a) compared to LSG (b) and HOPE (c).

11. Surface freshwater exchange (a) compared to the HOPE model (b).

12. Meridional heattransport as function of depth (a); Zonally averaged temperature in the Atlantic basin (b).

13. Zonally averaged temperature (a) and salinity (b) structure of the Southern Ocean.

14. Southern Hemisphere sea-ice coverage

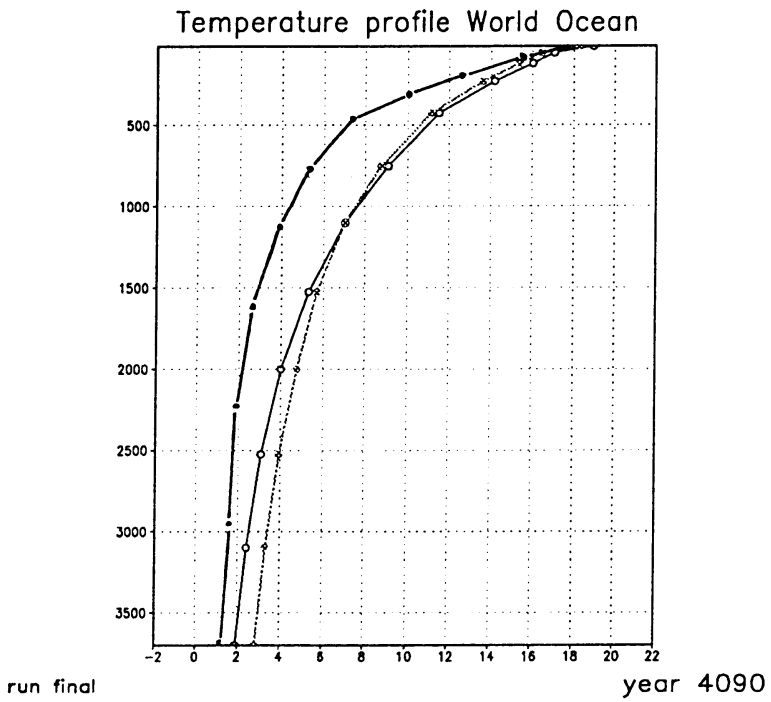
Temperature profile World Ocean
500
1000
1500
2000
2500
3000
3500
−2 0 2 4 6 8 10 12 14 16 18 20 22
run final
year 4090

1a

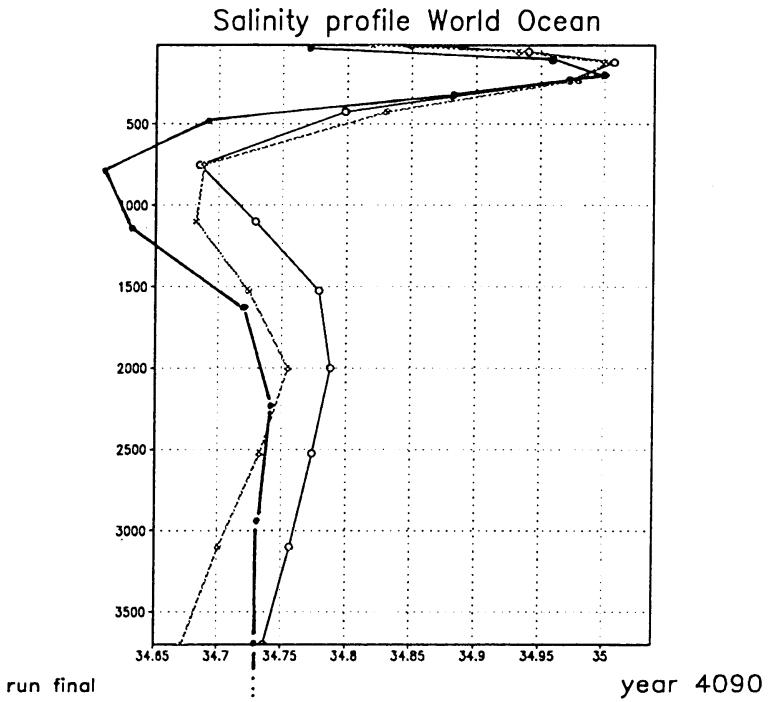
Salinity profile World Ocean
500
1000
1500
2000
2500
3000
3500
34.65 34.7 34.75 34.8 34.85 34.9 34.95 35
run final
year 4090

1b

2a Sigma–Theta; GEOSECS section West Atlantic (kg/m3)

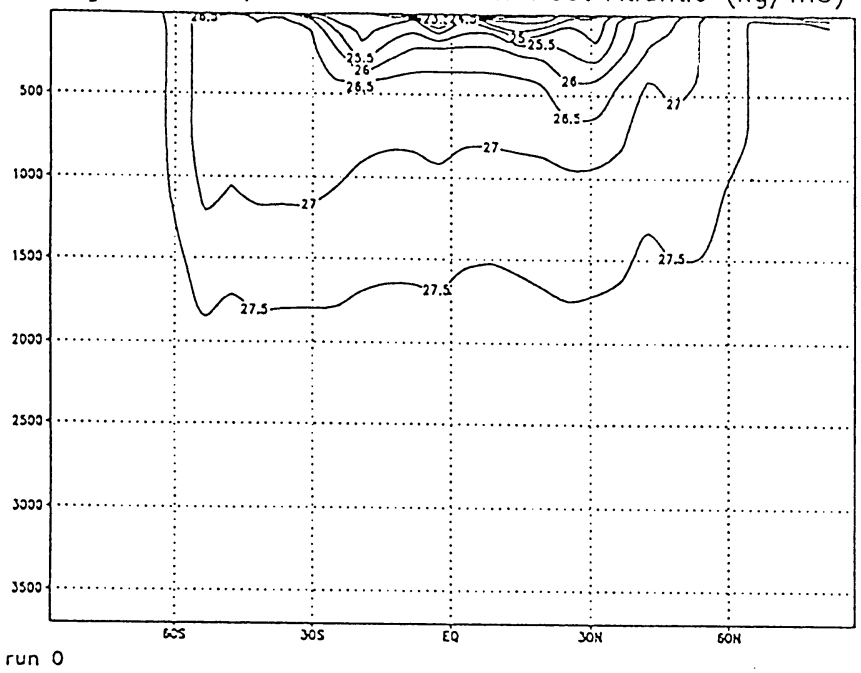

run 0

year 4090

2c

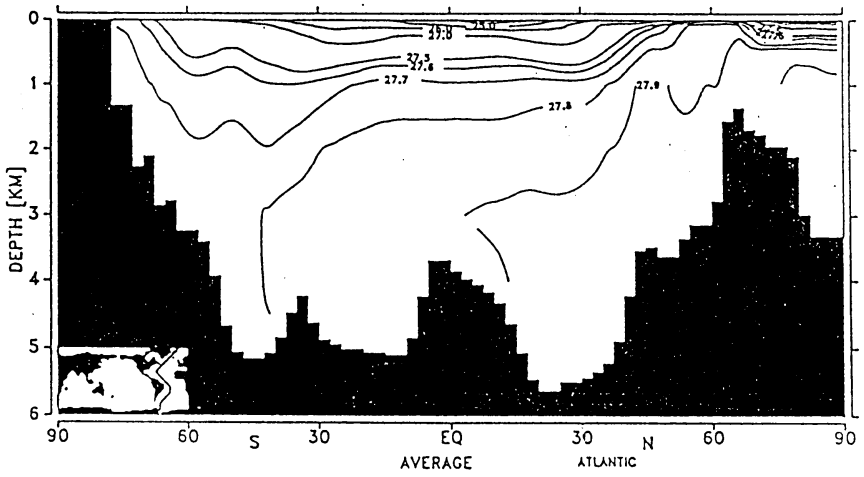

2e

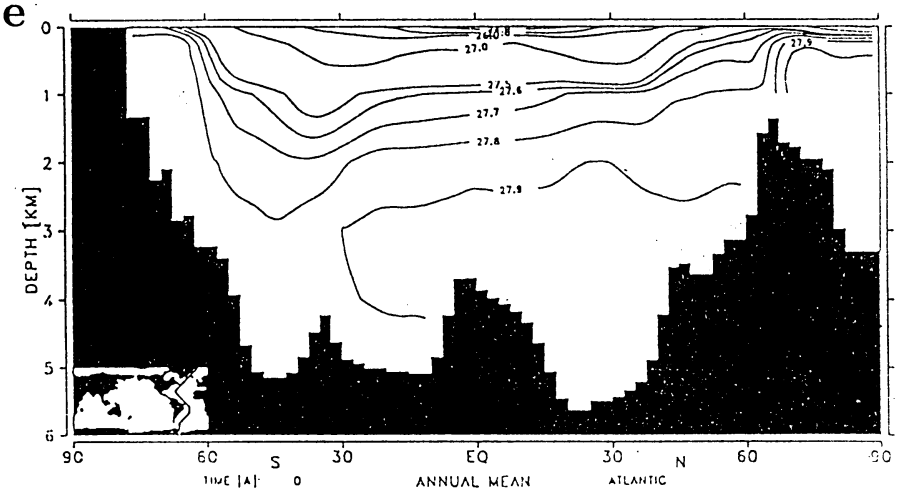

2b

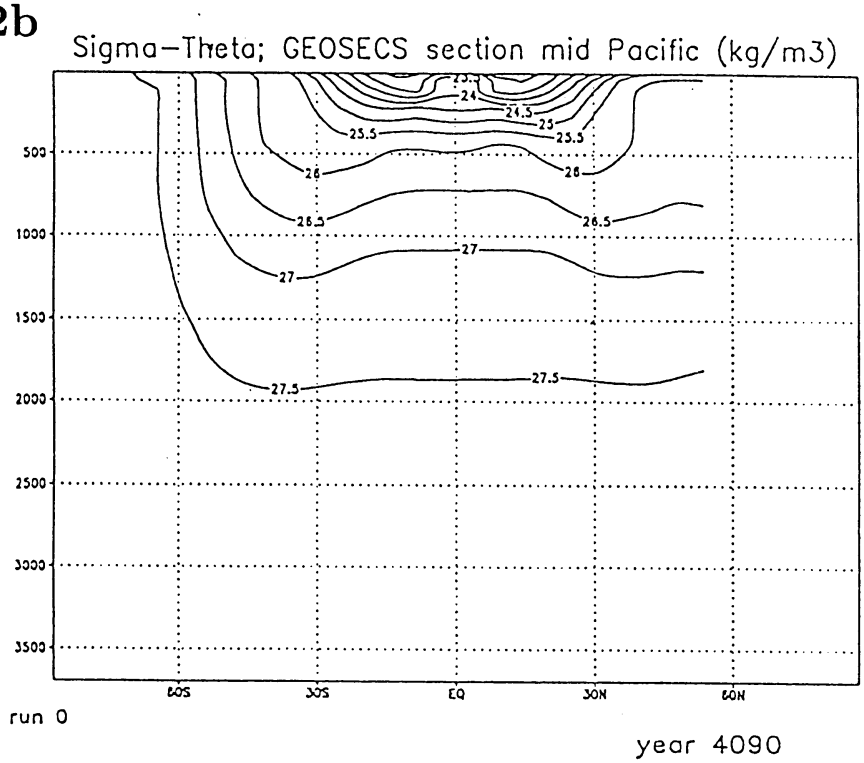
Sigma–Theta; GEOSECS section mid Pacific (kg/m3)
24
24.5
25
25.5
25.5
26
26
26.5
26.5
27
27
27.5
27.5
500
1000
1500
2000
2500
3000
3500
60S
30S
EQ
30N
60N
run 0
year 4090

2d

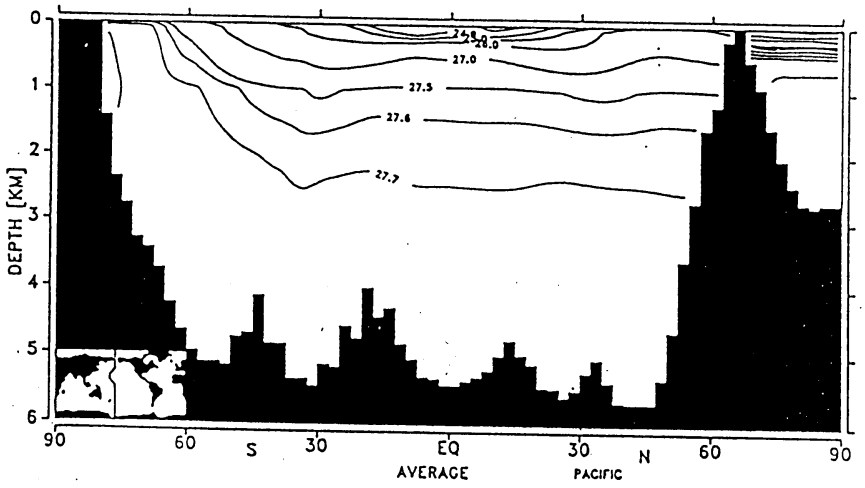
27.0
27.5
27.6
27.7
DEPTH [KM]
0
1
2
3
4
5
6
90
60
S
30
EQ
30
N
60
90
AVERAGE
PACIFIC

2f

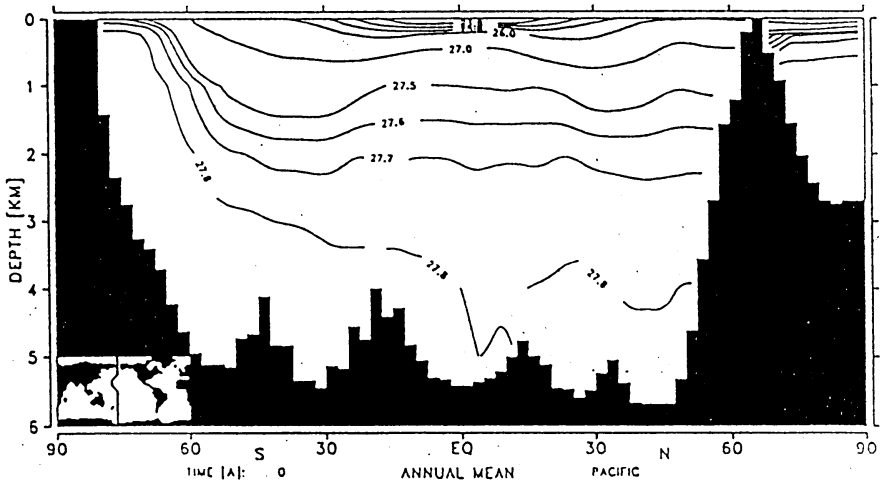
27.0
27.5
27.6
27.7
27.8
27.8
DEPTH [KM]
0
1
2
3
4
5
6
90
60
S
30
EQ
30
N
60
90
TIME [A]: 0
ANNUAL MEAN
PACIFIC

3a

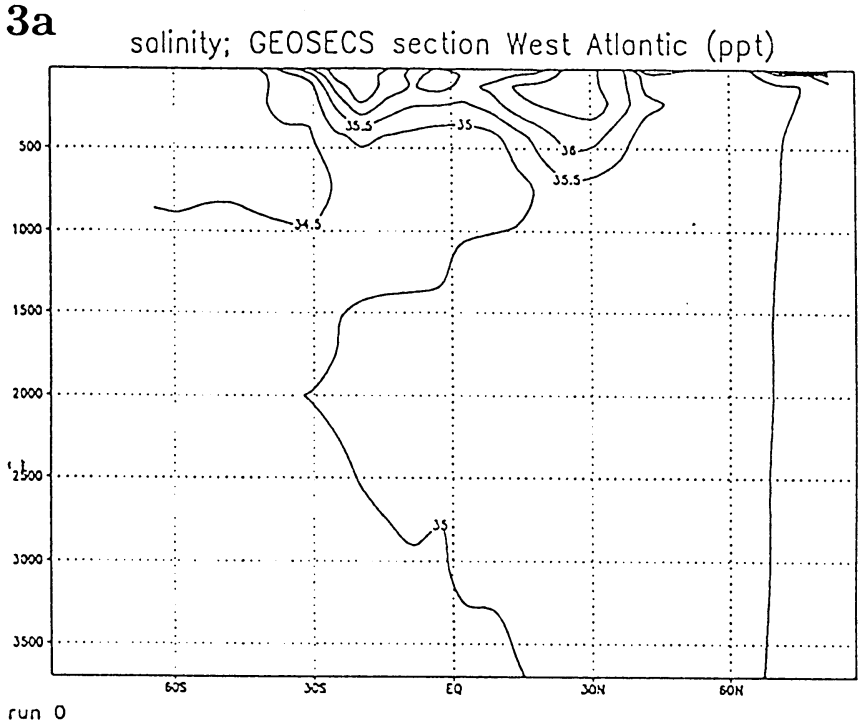

run 0

3c

year 4090

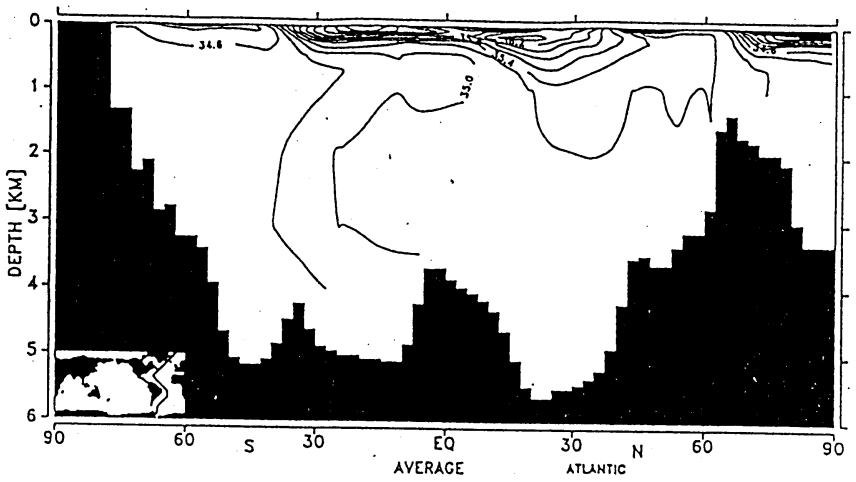

3e

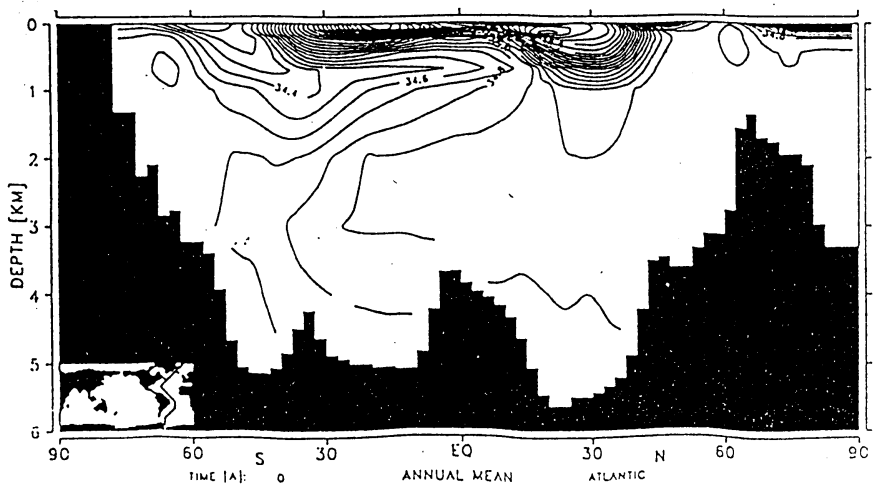

3b

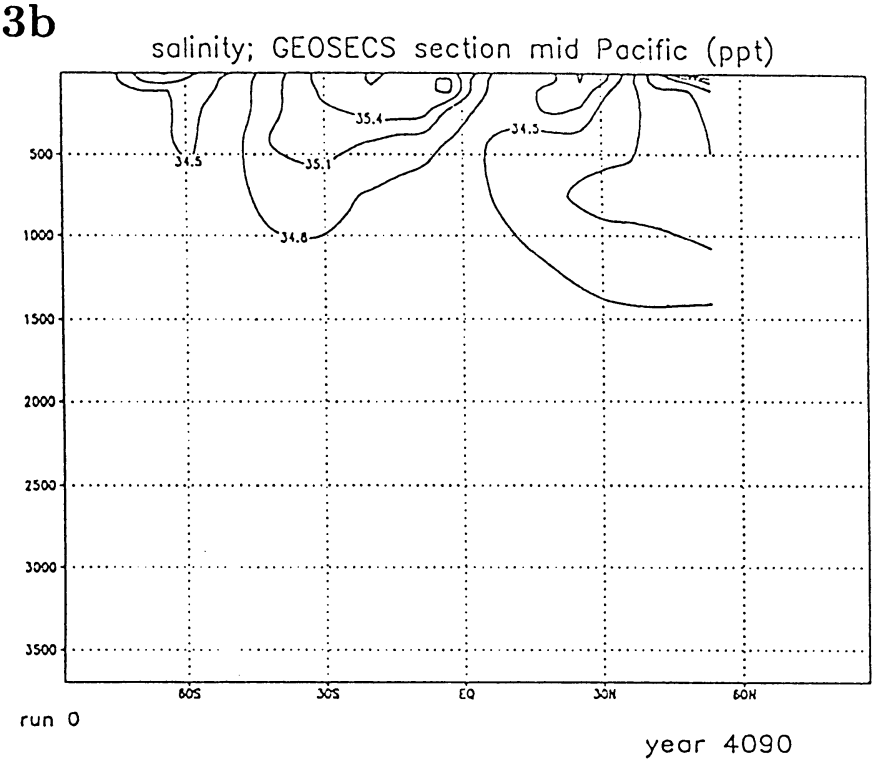
salinity; GEOSECS section mid Pacific (ppt)
35.4
34.5
34.5
35.1
34.8
500
1000
1500
2000
2500
3000
3500
60S
30S
EQ
30N
60N
run 0
year 4090

3d

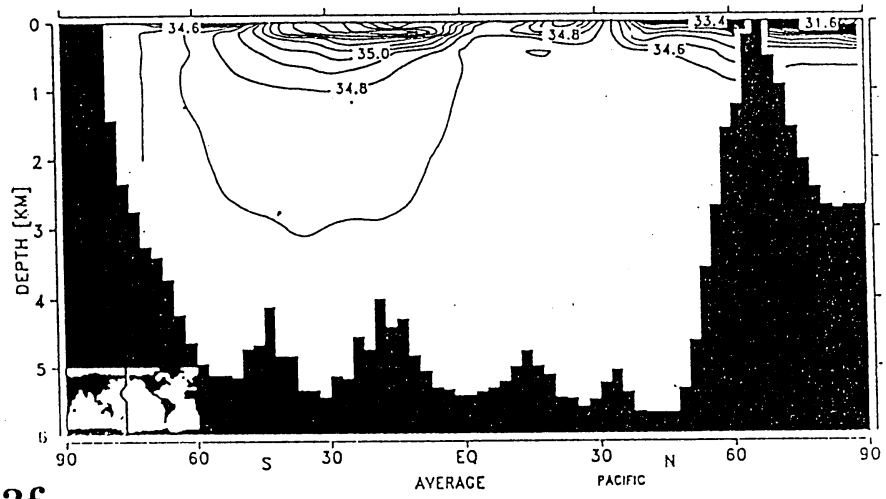
34.6
35.0
34.8
34.8
34.6
33.4
31.6
DEPTH [KM]
0
1
2
3
4
5
6
90
60
S
30
EQ
30
N
60
90
AVERAGE
PACIFIC

3f

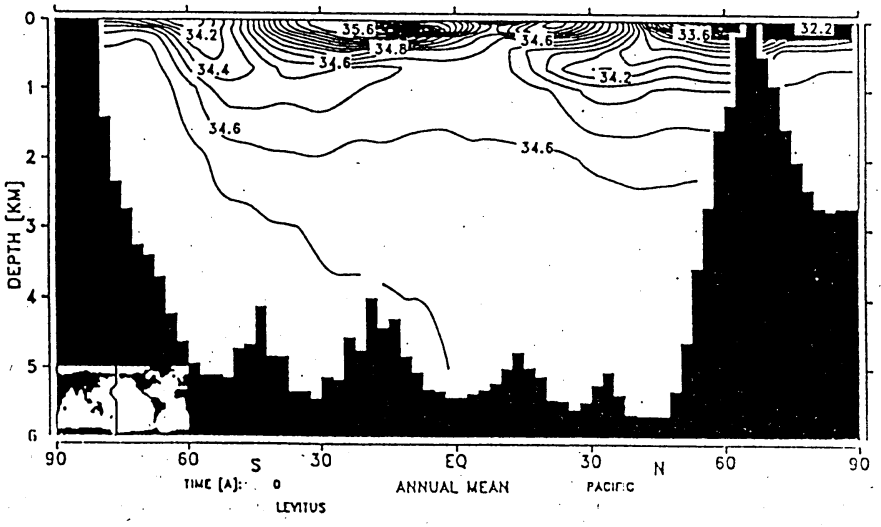
34.2
35.6
34.8
34.6
33.6
32.2
34.4
34.6
34.2
34.6
34.6
DEPTH [KM]
0
1
2
3
4
5
6
90
60
S
30
EQ
30
N
60
90
TIME [A]: 0
LEVITUS
ANNUAL MEAN
PACIFIC

4

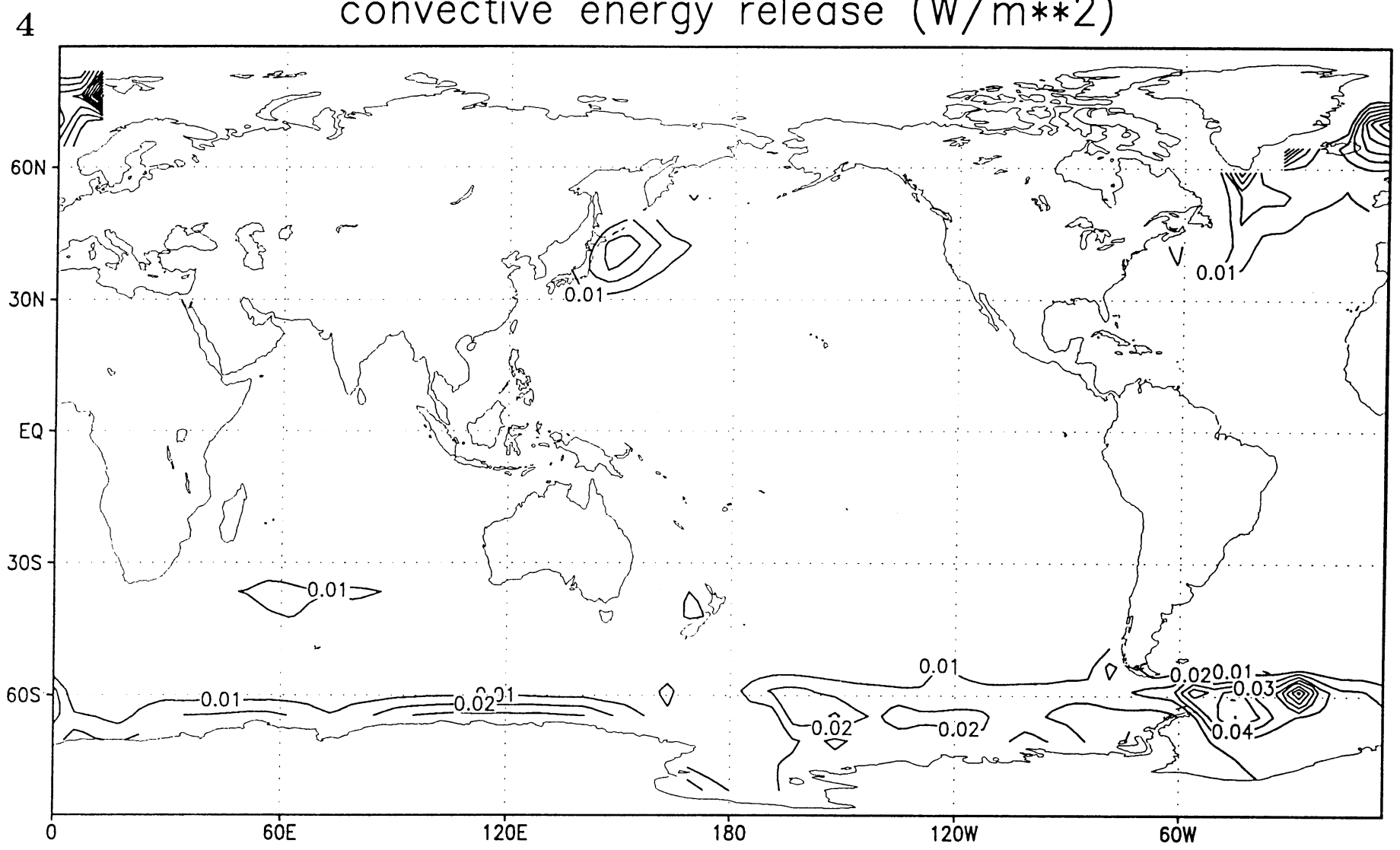
convective energy release (W/m**2)
60N
30N
EQ
30S
60S
0
60E
120E
180
120W
60W
0.01
0.01
0.01
0.01
0.02
0.01
0.01
0.02
0.02
0.02
0.01
0.03
0.04

velocities

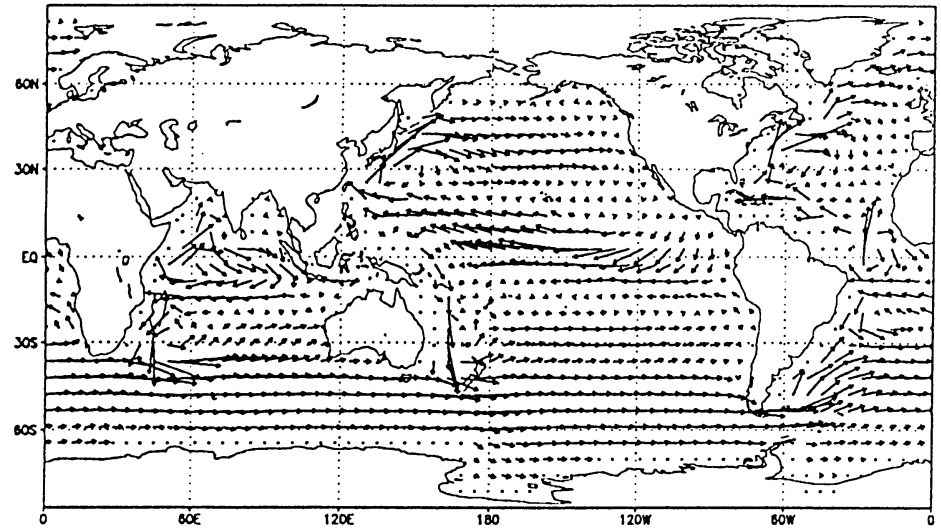

run 0

55 m (lev 2)
year 4090

velocities

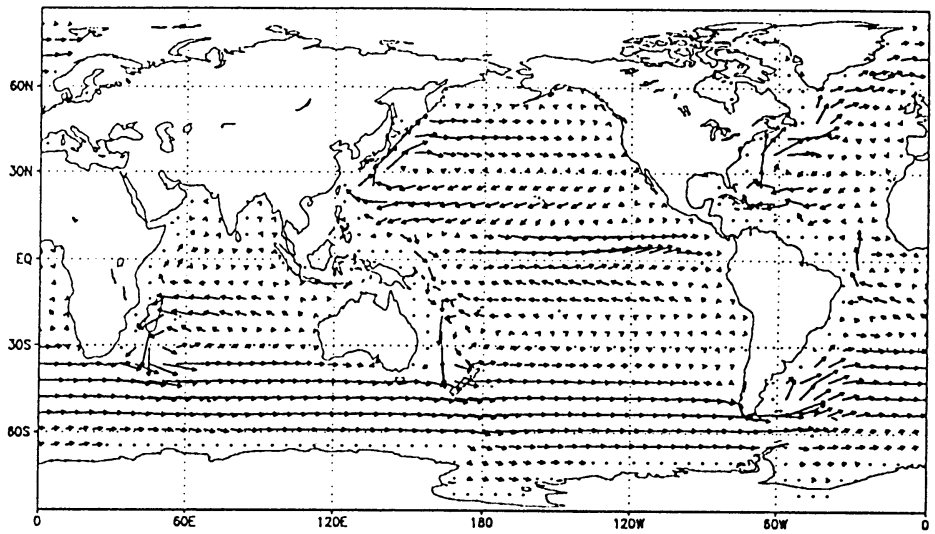

run 0

230 m (lev 4)
year 4090

velocities

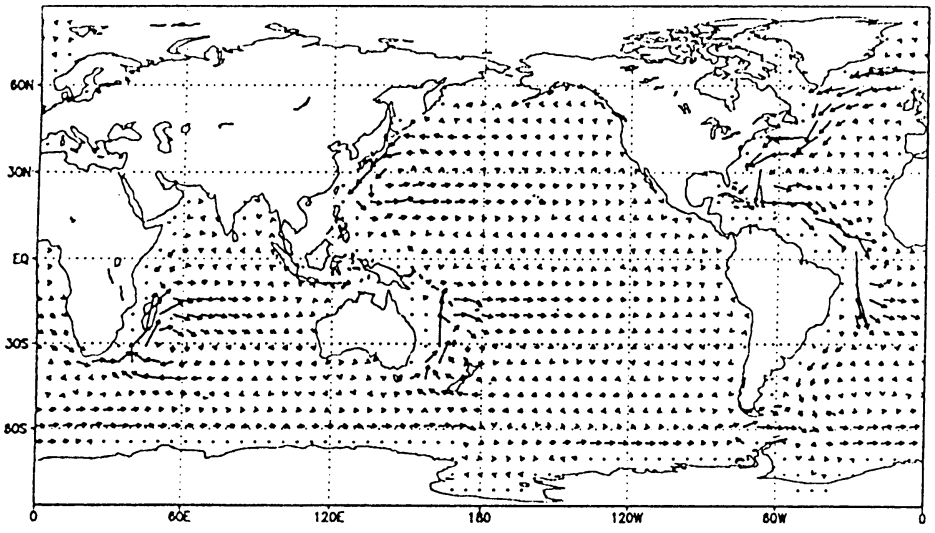

run 0

2000 m (lev 9)
year 4090

velocities

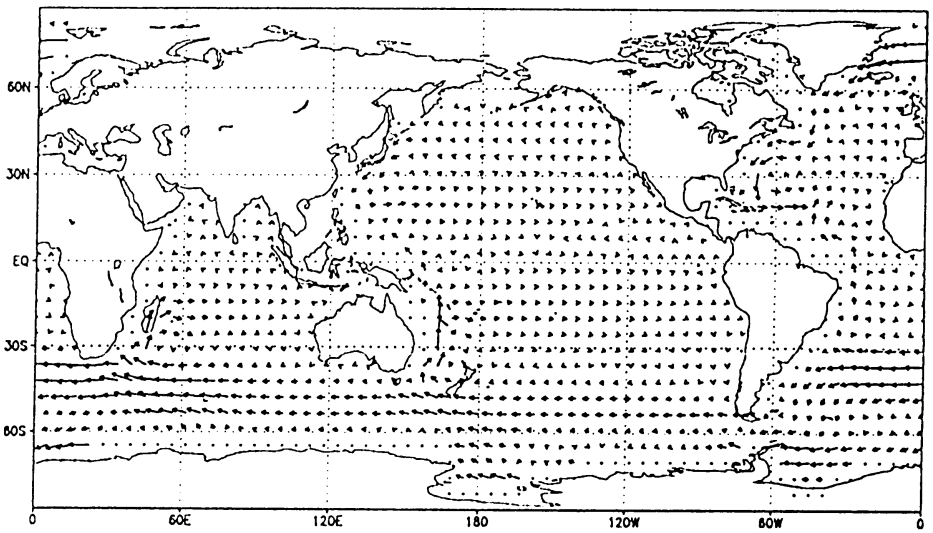

run 0

3700 m (lev 12)
year 4090

6a barotropic stream function (Sv)

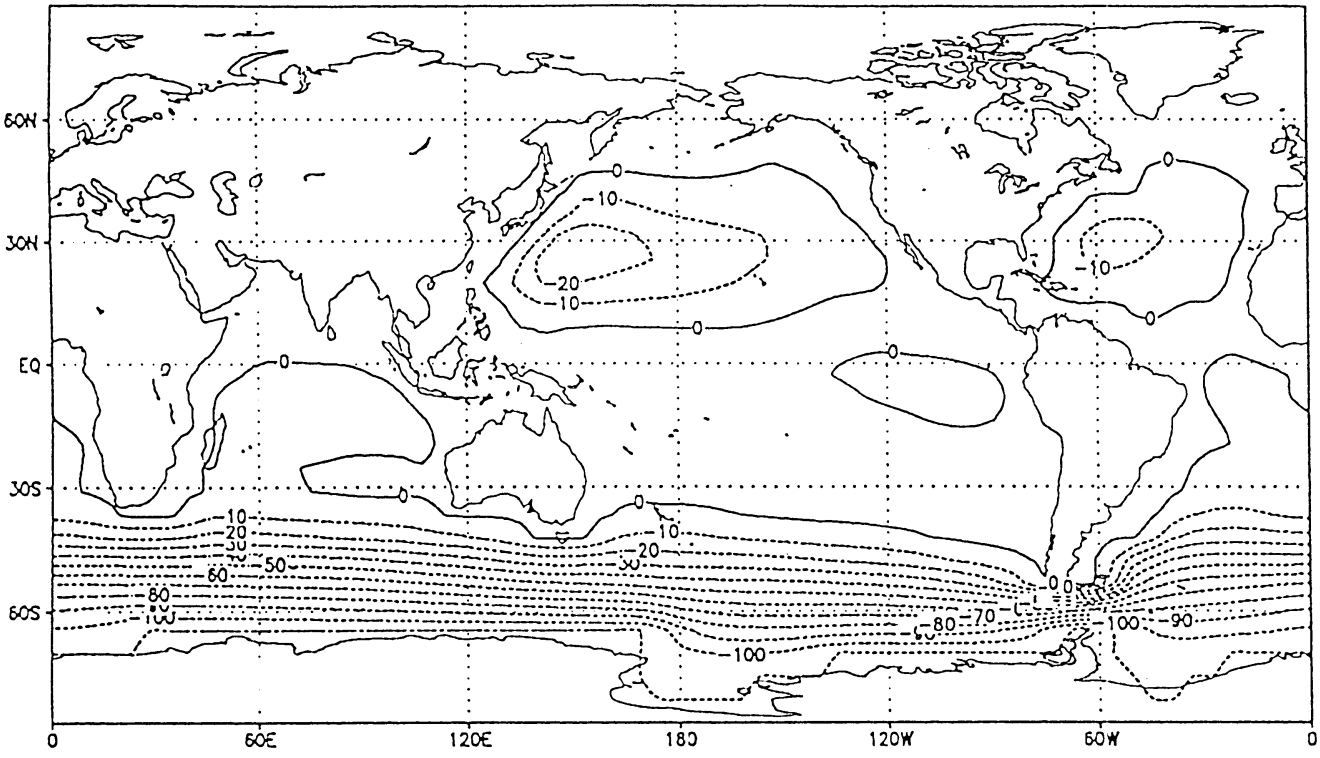

run 0

year 4090

6b

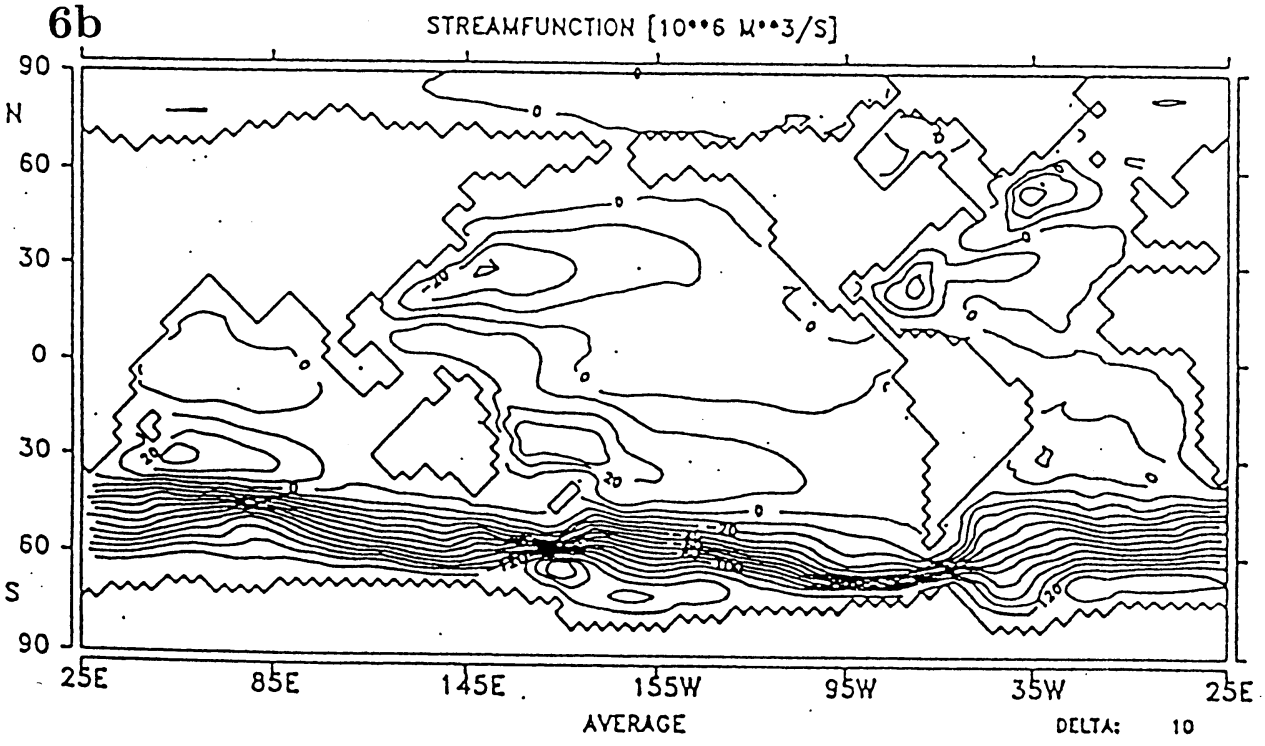

7a overturning Atlantic (Sv)

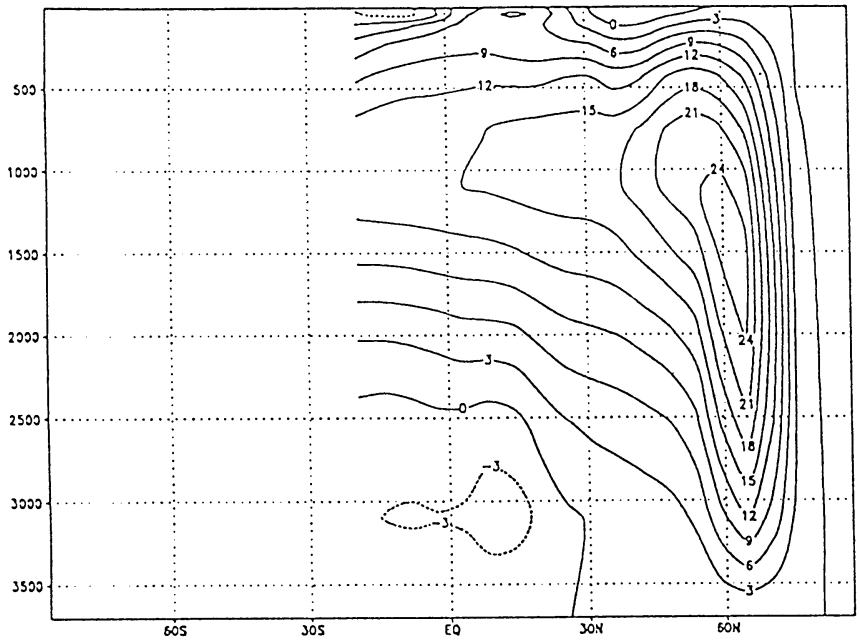

run SHice–Clim year 4090

7d

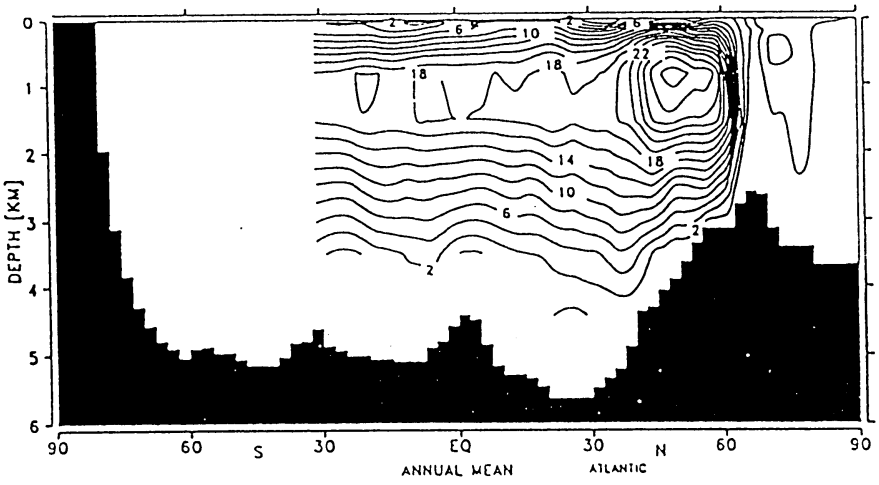

7b

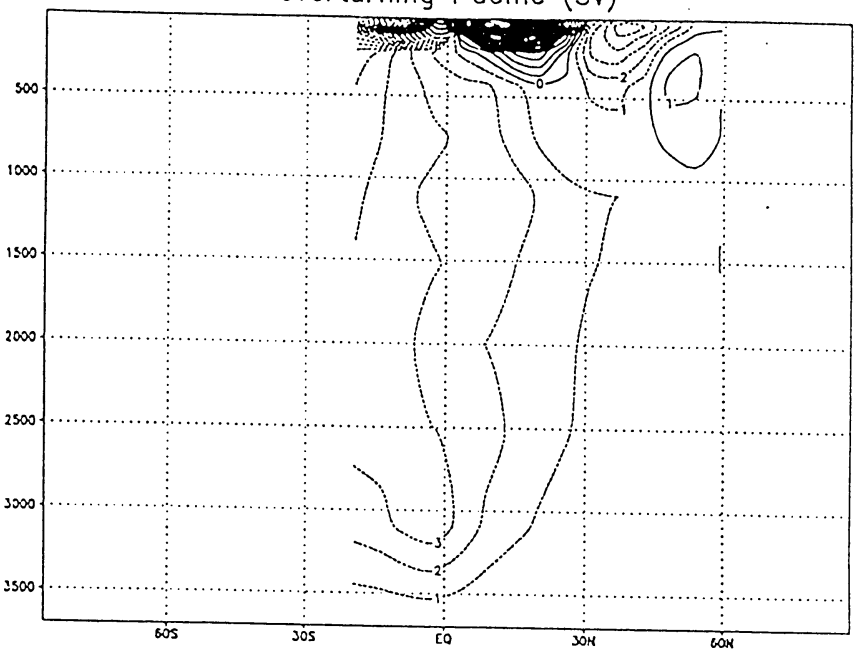
overturning Pacific (Sv)
500
1000
1500
2000
2500
3000
3500
60S
30S
EQ
30N
60N

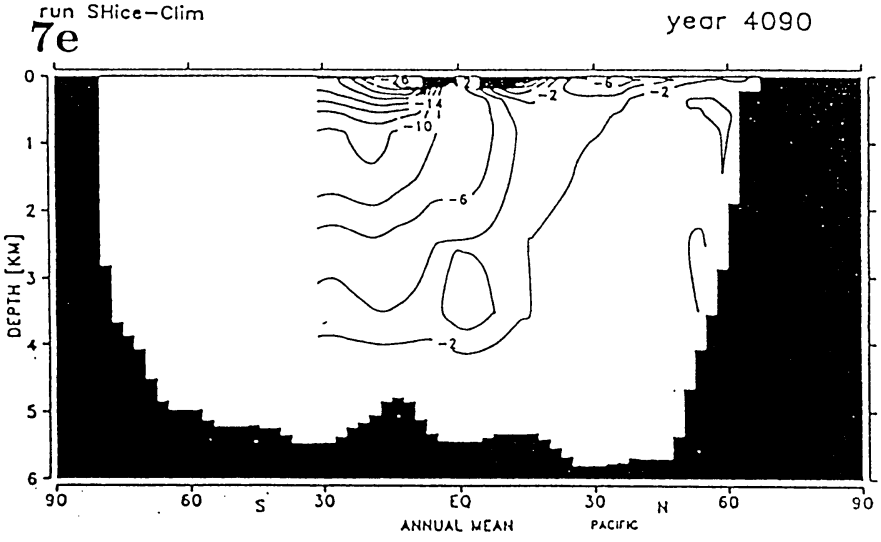
run SHice-Clim
year 4090
7e
DEPTH [KM]
0
1
2
3
4
5
6
90
60
S
30
EQ
30
N
60
90
ANNUAL MEAN
PACIFIC

7c

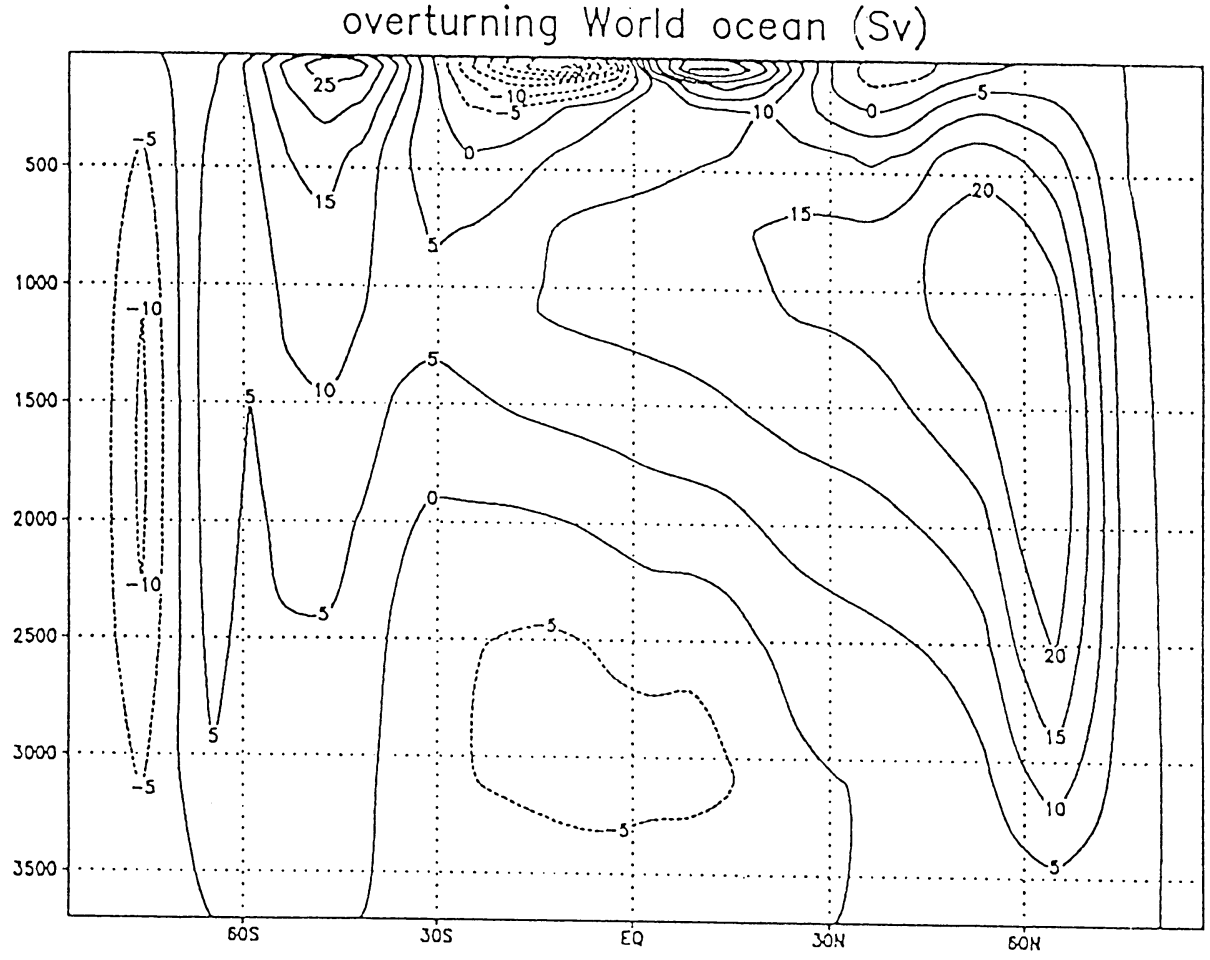

run SHice–Clim

year 4090

7e

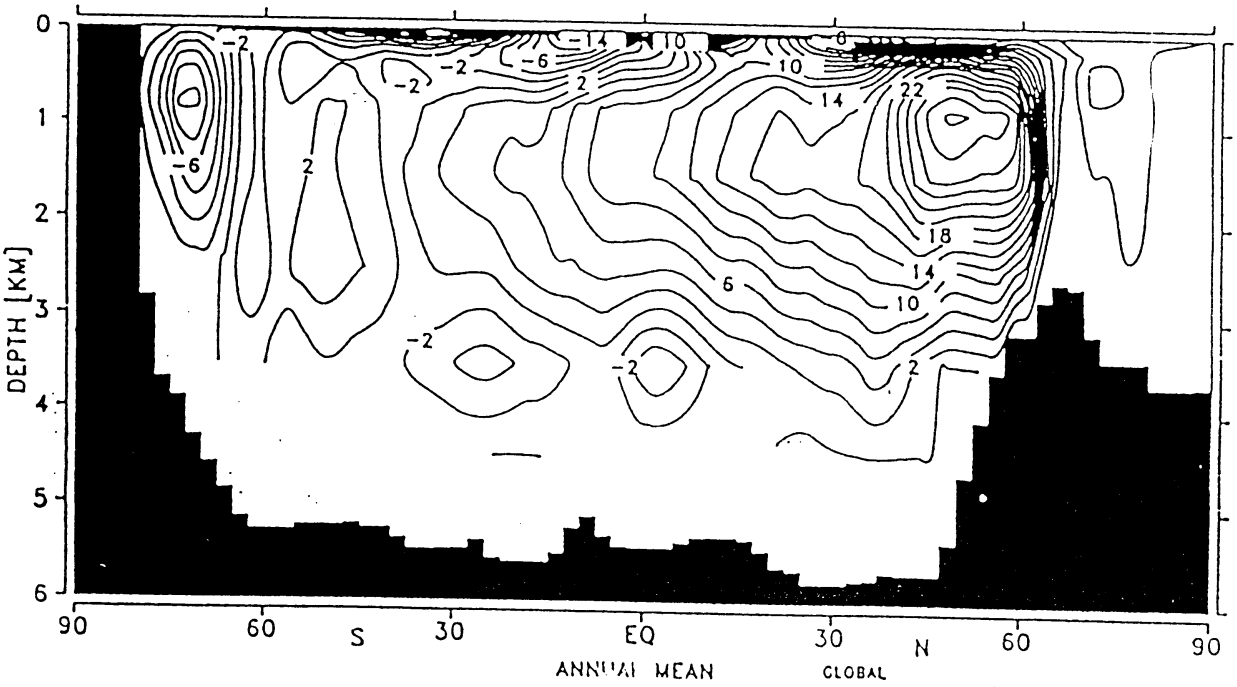

8a

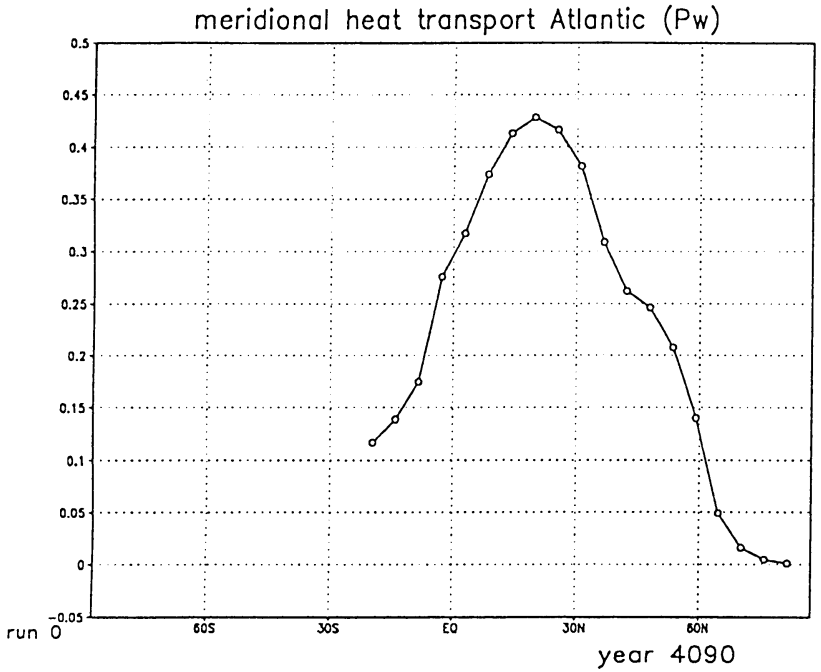
meridional heat transport Atlantic (Pw)
0.5
0.45
0.4
0.35
0.3
0.25
0.2
0.15
0.1
0.05
0
-0.05
60S
30S
EQ
30N
60N
run 0
year 4090

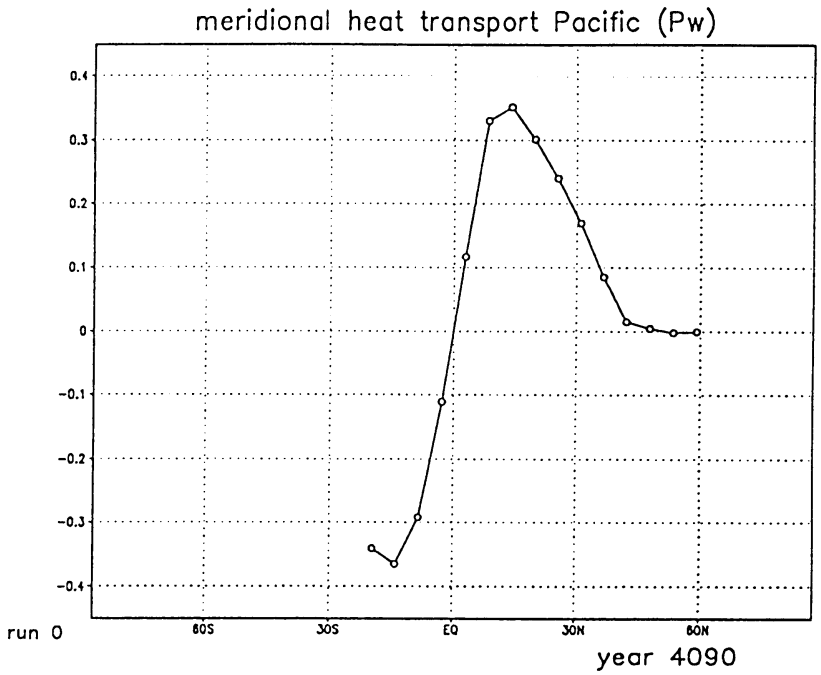
meridional heat transport Pacific (Pw)
0.4
0.3
0.2
0.1
0
-0.1
-0.2
-0.3
-0.4
60S
30S
EQ
30N
60N
run 0
year 4090

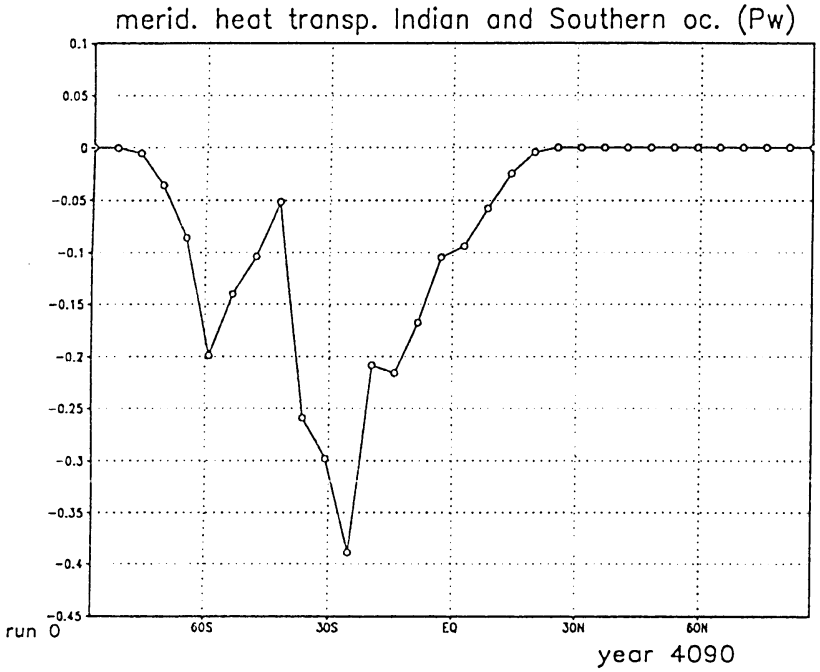
merid. heat transp. Indian and Southern oc. (Pw)
0.1
0.05
0
-0.05
-0.1
-0.15
-0.2
-0.25
-0.3
-0.35
-0.4
-0.45
60S
30S
EQ
30N
60N
run 0
year 4090

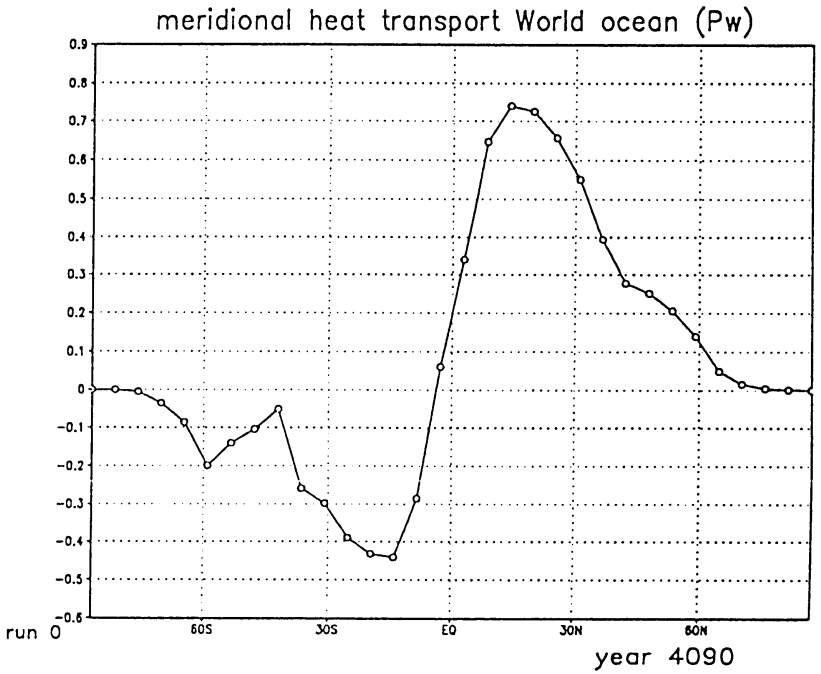
meridional heat transport World ocean (Pw)
0.9
0.8
0.7
0.6
0.5
0.4
0.3
0.2
0.1
0
-0.1
-0.2
-0.3
-0.4
-0.5
-0.6
60S
30S
EQ
30N
60N
run 0
year 4090

8b

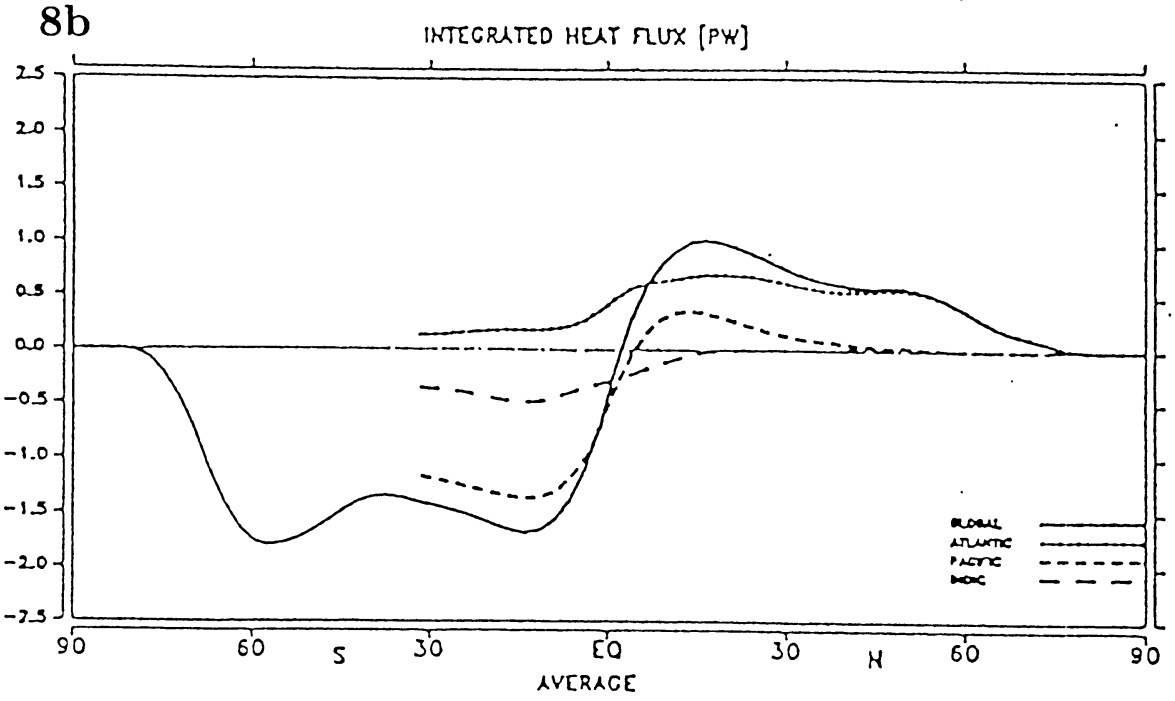

AVERAGE

8c

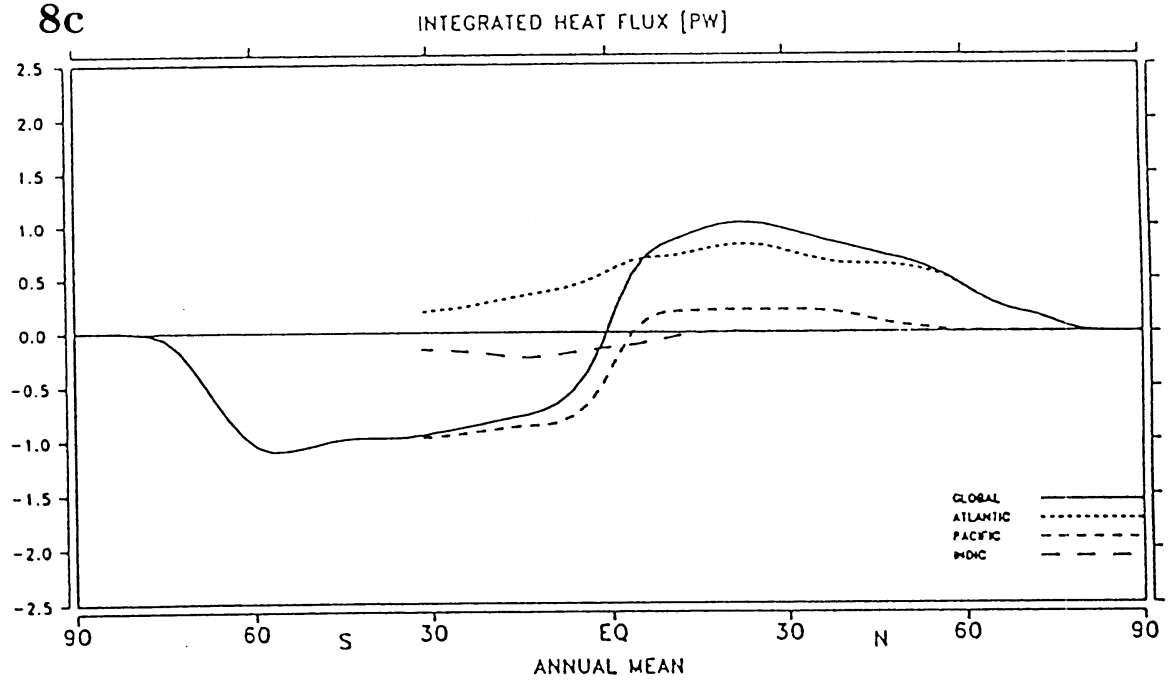

ANNUAL MEAN

9a

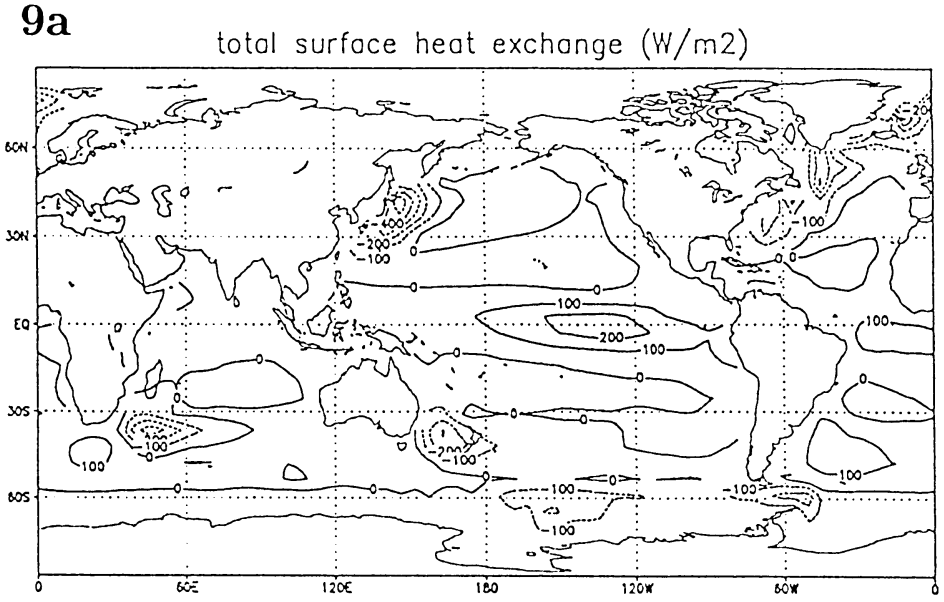
total surface heat exchange (W/m2)
60N
30N
EQ
30S
60S
0
60E
120E
180
120W
60W
0
run 0
year 4090

9b

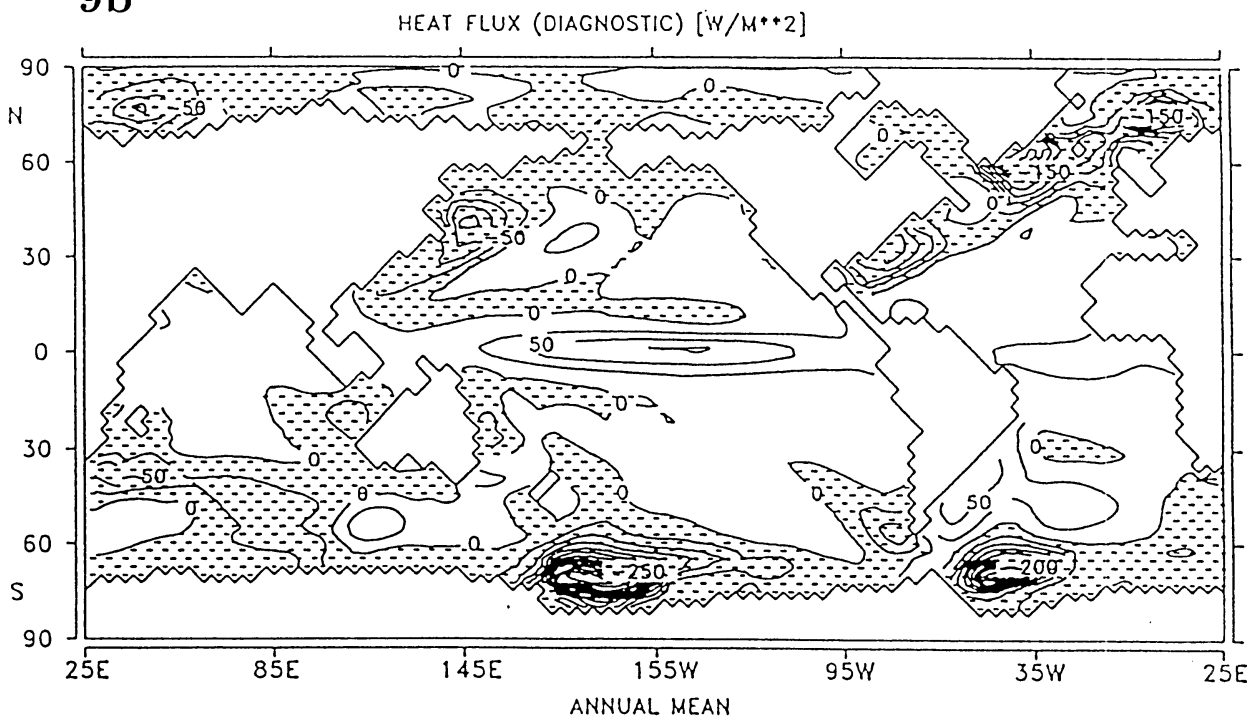
HEAT FLUX (DIAGNOSTIC) [W/M**2]
90
N
60
30
0
30
60
S
90
25E
85E
145E
155W
95W
35W
25E
ANNUAL MEAN

10a

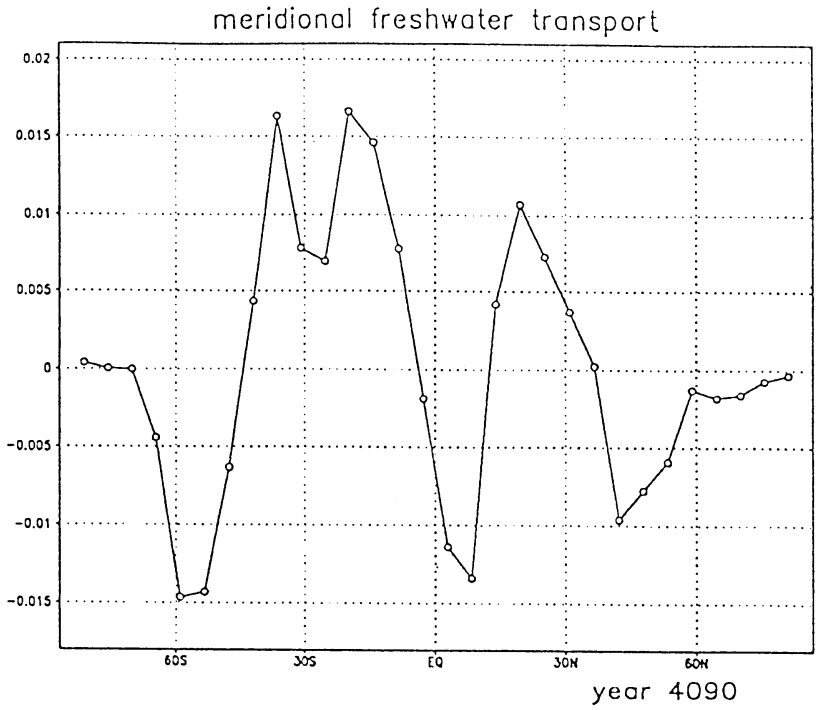
meridional freshwater transport
0.02
0.015
0.01
0.005
0
-0.005
-0.01
-0.015
60S
30S
EQ
30N
60N
year 4090

10b

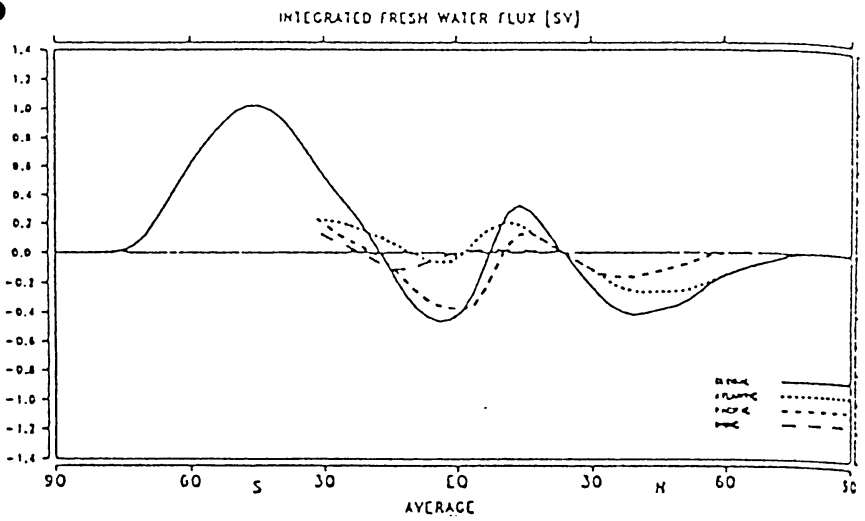
INTEGRATED FRESH WATER FLUX [SV]
90
60
S
30
EQ
30
N
60
AVERAGE

10c

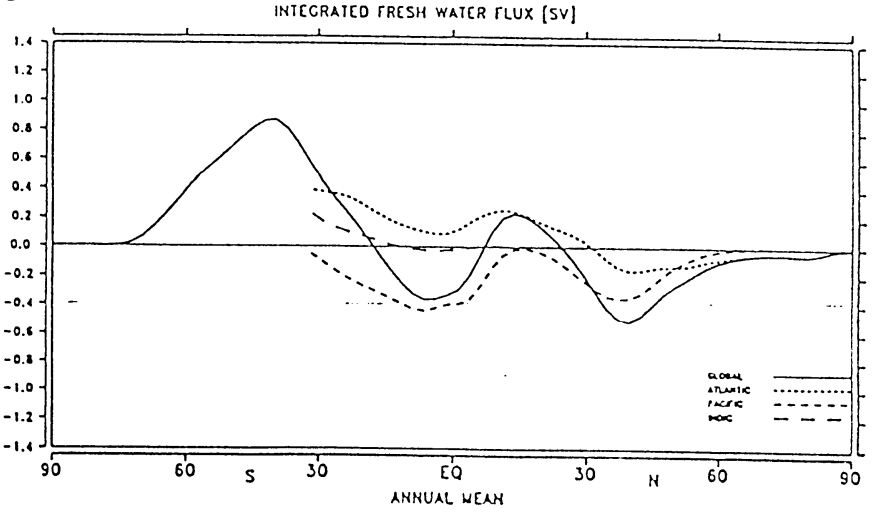
INTEGRATED FRESH WATER FLUX [SV]
90
60
S
30
EQ
30
N
60
90
ANNUAL MEAN

11a

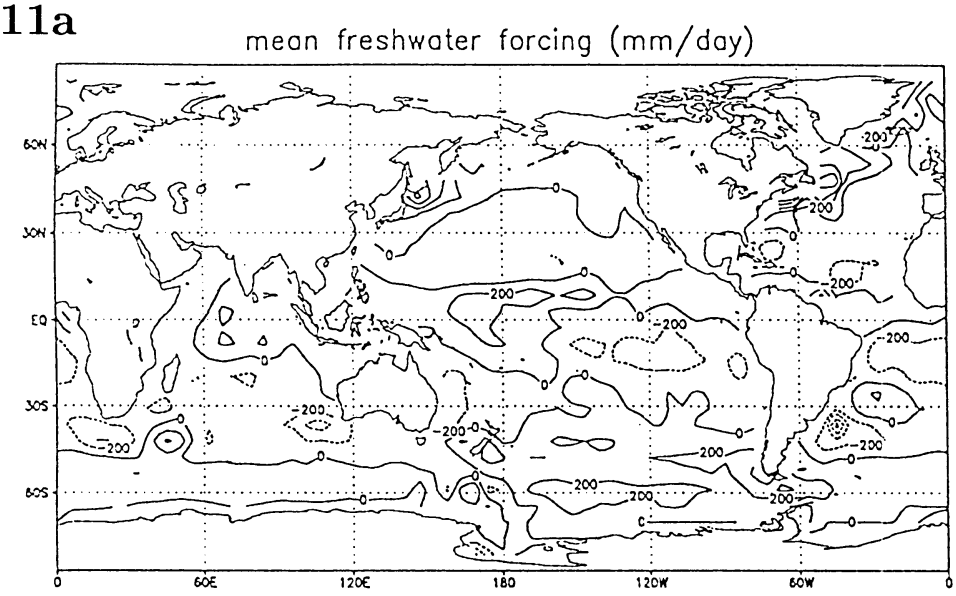

run 0

year 4090

11b

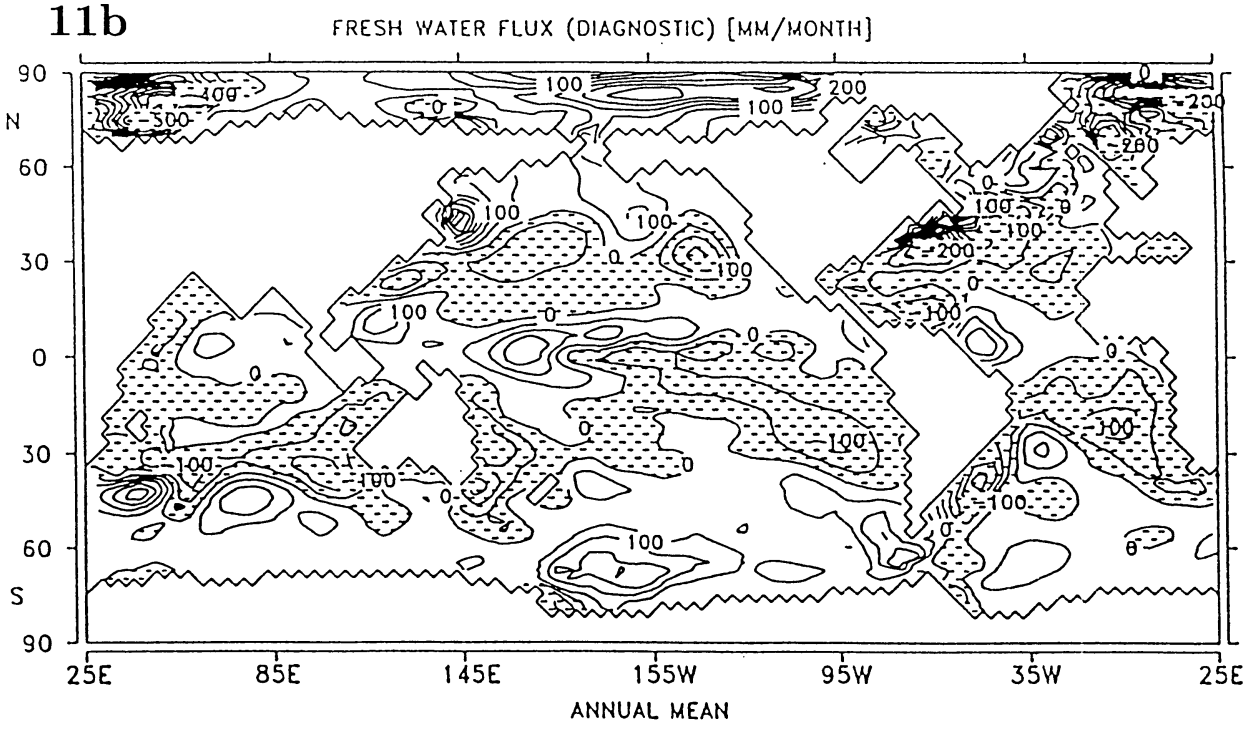

12a meridional heat transport Atlantic (Pw)

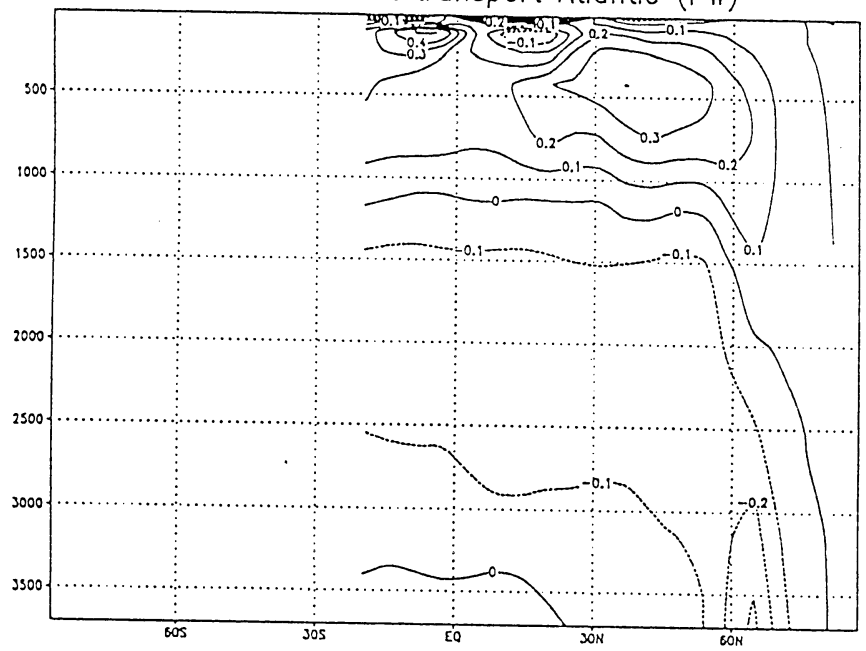

run SHice–Clim

year 4090

12b zonal average temperature Atlantic (C)

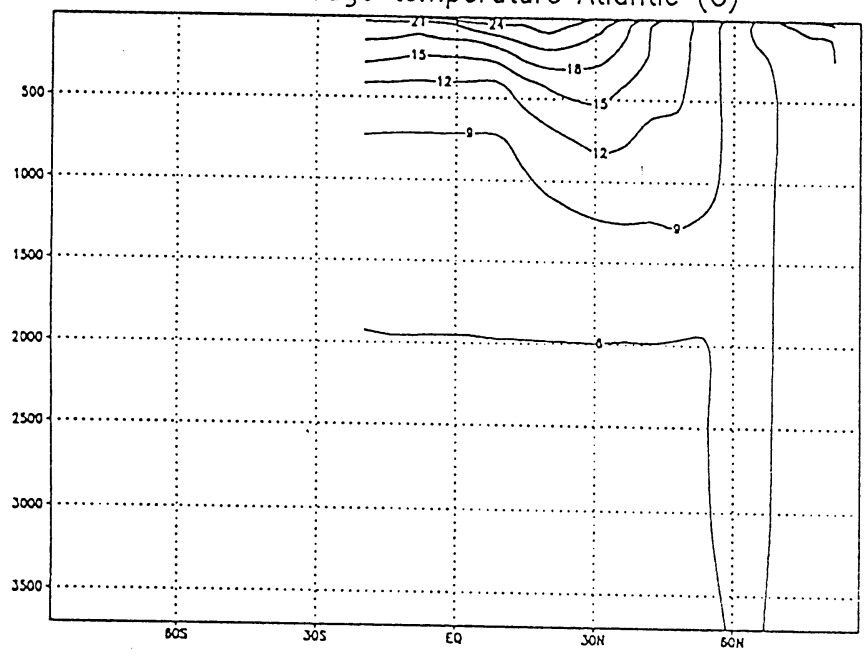

run SHice–Clim

year 4090

13a

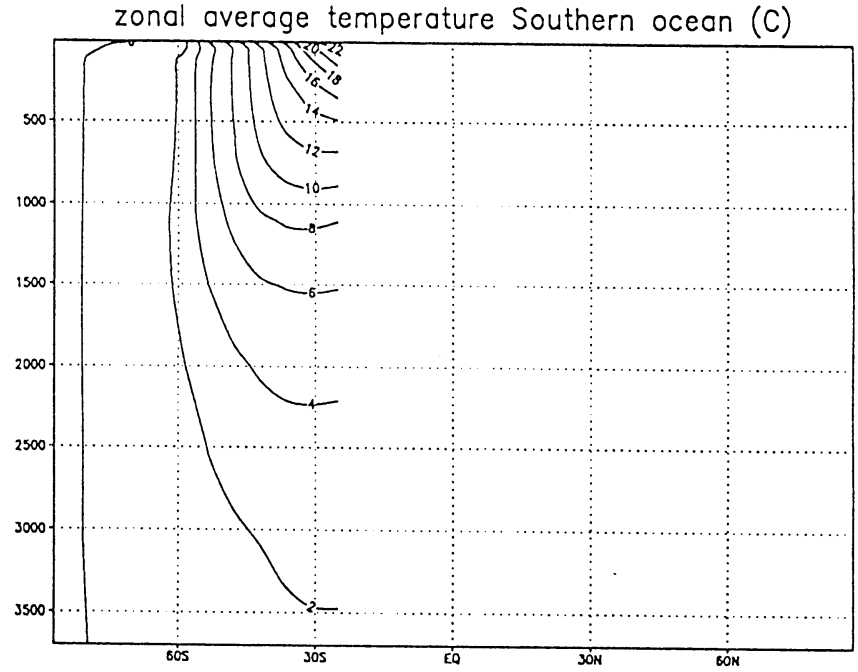

run 0

year 4090

13b

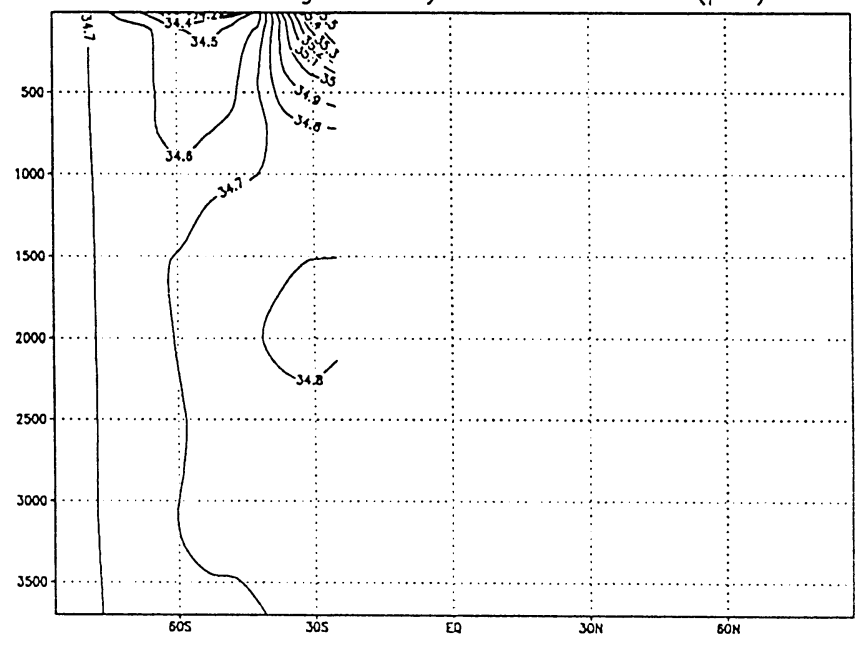

run 0

year 4090

SH ice coverage